Bergische Universität Wuppertal

Fakultät für Mathematik und Naturwissenschaften

Institute of Mathematical Modelling, Analysis and Computational Mathematics (IMACM)

Preprint BUW-IMACM 22/02

Hanno Gottschalk, Nicolai Rothe und Daniel Siemssen

Special cosmological models derived from the semiclassical Einstein equation on flat FLRW space-times

January 5, 2022

http://www.imacm.uni-wuppertal.de

Special cosmological models derived from the semiclassical Einstein equation on flat FLRW space-times

Hanno Gottschalk*, Nicolai Rothe* and Daniel Siemssen*

*School of Mathematics and Natural Science & IMACM,

University of Wuppertal, D-42119 Wuppertal, Germany

{gottschalk,rothe,siemssen}@uni-wuppertal.de

January 5, 2022

This article presents numerical work on a special case of the cosmological semiclassical Einstein equation (SCE). The SCE describes the interaction of relativistic quantum matter by the expected value of the renormalized stress-energy tensor of a quantum field with classical gravity. Here we consider a free massless scalar field with general (not necessarily conformal) coupling to curvature. In a cosmological scenario with flat spatial sections for special choices of the initial conditions, we observe a separation of the dynamics of the quantum degrees of freedom from the dynamics of the scale factor, which extends a classical result by Starobinsky [40] to general coupling. For this new equation of fourth order for the dynamics of the scale factor, we study numerical solutions. Typical solutions show a radiation-like Big Bang for the early universe and de Sitter-like expansion for the late universe. We discuss a specific solution to the cosmological horizon problem that can be produced by tuning parameters in the given equation. Although the model proposed here only contains massless matter, we give a preliminary comparison of the obtained cosmology with the ΛCDM standard model of cosmology and investigate parameter ranges in which the new models to a certain extent assimilates standard cosmology.

Key words: Semiclassical Einstein equation • cosmology • higher derivative gravity • asymptotic de Sitter solutions

1 Introduction

This paper introduces a new set of cosmological equations that emerge as a special case from the semiclassical Einstein equation (SCE). The SCE is proposed as a minimal modification to general relativity that takes quantum matter into account, see e.g. [7, 16, 22, 42]. While the SCE is generally not believed to be a fundamental theory, it is widely studied in situations where the relevant physics takes place on scales that are well separated from Planck scale and in cosmological scenarios [39]. Many special or approximate cosmological solutions to the SCE have been reported [9, 15, 15, 25, 26, 40].

The mathematical understanding of the SCE has only advanced recently for the case of cosmological applications [18, 31, 35, 36]. The intrinsic reason for the difficulties in formulating the

SCE in a mathematically consistent fashion lie in the higher derivatives that occur by the covariant renormalization of the stress-energy tensor [24, 32] that lead to an implicit definition of the dynamical system that describes the SCE [13]. In [18], however, the dynamical degrees of freedom of the quantum field were redefined using certain expansions of the two point functions of the quantum field in homogeneous distributions as renormalization scheme and inserting correction terms in order to guarantee the equivalence with the standard Hadamard point splitting renormalization. In this way one obtains a formulation of the cosmological SCE as an explicit, infinite-dimensional dynamical system. The (infinitely many) dynamic degrees of freedom of the quantum field here enter via the prefactors of the aforementioned expansion and are organized in a 'tower of moments'. In particular, this is possible for arbitrary (not necessarily conformal) coupling of the quantized field to the scalar curvature.

The present paper is based on a crucial observation, namely that (a) the dynamic equation for the tower of moments is linear homogeneous and (b) there are massless physical states for all (not necessarily conformal) couplings with vanishing moments as initial conditions. As a homogeneous linear equation maps zero initial data to the vanishing solution, the dynamics of the quantum field effectively decouples from the dynamics of the scale factor. We therefore derive a fourth order system of equations for the scale factor where quantum effects only enter via geometric terms. This extends the classical Starobinsky cosmologies for the conformal coupling [40] to general couplings.

This paper is devoted to the description and the detailed numerical investigation of this new system of cosmological equations. In particular, we review the derivation and the special assumptions which these equations are based on, we give a few examples of explicit solutions for certain settings of the parameters including Minkowski and de Sitter-phases and also discuss approximate solutions that relate to higher order gravity [6, 14]. These latter approximate solutions incorporate both a radiation like Big Bang with a slow-down in expansion speed and a re-acceleration phase prior to an asymptotic de Sitter phase for the late universe. We thereafter provide numerical evidence that for large regions of the parameter space the numerical solutions for generic parameter settings reproduce this behavior.

We furthermore provide a numerical exploration of solutions in dependence of the parameters. Among these solutions we highlight a subset that relates to a solution of the cosmological horizon problem proposed by N. Pinamonti [35] and based on the diverging negative conformal time for the Big Bang.

We also discuss parameter settings that assimilate solutions to our equations to solutions of the ΛCDM standard model of cosmology. This is done for two reasons: On the one hand this can be seen as a case study about how flexible cosmological models from the SCE can be and to anticipate features of more realistic SCE-cosmologies that involve more realistic forms of matter and not only massless scalar quantum fields. On the other hand, we wish to identify some preliminary ideas on the order of magnitude of parameters that enter the SCE. Here we apply the ΔN_{eff}-test proposed by T. Hack as a test for the SCE at redshift factor $z = 3000$, corresponding to the emission of the cosmic microwave background [22]. In particular, interesting parameter regions seem to be close (but not restricted) to conformal coupling $\xi = \frac{1}{6}$. These first insights of course require confirmation from models with more realistic composition of matter.

The qualitative results presented in our paper are in line with prior analytical and numerical work by other authors. While the Minkowski solution to the SCE is obvious, de Sitter phases for conformal coupling and massless fields have been found by A. A. Starobinsky [40]. Recently, special solutions of de Sitter type have been found by B. A. Juaréz for massless and massive quantum a3[8fields for special settings of parameters in the Bunch-Davies vacuum state [25]. Here we find further such solutions for special parameter sets of our new model's equations that lead to de Sitter type expansion [17].

Asymptotically de Sitter solutions without introducing a cosmological constant have been observed e.g. in [9] for a dynamical system derived from the SCE with a massive quantum field for conformal coupling and approximate KMS-like states, see also the in-depth discussion in [22] (and references therein) and the recent study of M. Hänsel [23] on the phase diagram of the massless SCE with conformal coupling. All these works, however, are restricted to conformal coupling, whereas, in the present article, we extend this type of results to non conformal coupling.

Prior work on the numerics of the SCE has been given by P. R. Anderson [2–5]. In contrast to our work, the quantum fields in the first three articles are only corrections to classical background fields. Here asymptotically classical solutions close to the Big Bang are found for generic values of the renormalization constants. As the numerics in these works is restricted to the very early universe shortly after the Big Bang, this is in line with our findings of a radiation like Big Bang for massless scalar fields (Anderson also treats massive fields). In [5], where no background fields is assumed, de Sitter solutions are found as well. The conformal *ansatz* to set initial conditions at the Big Bang is again restricted to $\xi = \frac{1}{6}$, which is not the case in our system.

Work on the comparison of SCE-cosmology with the ΛCDM model can be found in [15,20–22], again mostly for conformal coupling. Here, in particular, we employ similar methods for a parameter screening of the SCE for our special system of cosmological equations for more general coupling.

Our paper is organized as follows: In Section 2 we recapitulate the moment formulation of the SCE. Section 3 derives our special, decoupled cosmological models and proves that they lead to full solutions of the SCE. The subsequent Section 4 discusses special de Sitter solutions, the settings for initial conditions and parameters. Also, the state variable is introduced in order to compare the matter content generated by the quantum field with the matter content of perfect-fluid Friedmann-type cosmologies. Finally, Section 4 contains the first numerical results of this paper. In Section 5 we then provide parameter studies for numerical solutions and also include a short digression into the cosmological horizon problem. We furthermore show in Section 6 that our solutions can be fitted to the ΛCDM standard cosmology such that they completely lie in the uncertainty band of the ΛCDM model. Finally, we identify promising regions for parameters using the ΔN_{eff}-test as suggested in [22]. Section 7 gives our conclusions and some comments on future research.

2 The moment approach to the cosmological SCE

This section introduces our notation an briefly recapitulates the moment approach to the cosmological SCE as introduced in [18]. We consider the semiclassical Einstein equation

$$G_{\mu\nu} = \kappa \langle T^{\text{ren}}_{\mu\nu} \rangle_\omega \tag{1}$$

with the metric's sign convention $(-,+,+,+)$. Here $G_{\mu\nu}$ is the Einstein tensor and $\langle T^{\text{ren}}_{\mu\nu} \rangle_\omega$ is the renormalized stress-energy tensor of a free, scalar and chargeless quantum field. The field dynamics is given by the Klein-Gordon (KG) equation,

$$\left[\Box + m^2 + \xi R\right] \phi = 0, \tag{2}$$

where $\Box = -g^{\mu\nu}\nabla_\nu\nabla_\mu$ is the d'Alambertian associated with the Levi-Civita connection ∇ for the Lorentzian metric $g_{\mu\nu}$. $\xi \in \mathbb{R}$ parameterizes the curvature coupling and $m \geq 0$ defines the field's mass. The special case $\xi = \frac{1}{6}$ is referred to as conformal coupling. Let $G_{\text{ret/adv}}$ be the retarded and advanced fundamental solutions to the KG-equation, then ϕ is quantized such that it fulfills the canonical commutation relations (CCR) $[\phi(x), \phi(y)] = i\,(G_{\text{ret}}(x,y) - G_{\text{adv}}(x,y))$, see e.g. [11, 12, 16, 42]. Note that with ϕ, also $\alpha\phi$ for $\alpha \in \mathbb{R} \setminus \{0\}$ is another legitimate local

quantum field. By the CCR in the given shape, we are normalizing the field strength to $\alpha = 1$ and we obtain $\kappa = 8\pi G_N \alpha^2$, where G_N is Newton's gravitational constant. The field strength remains as a free parameter of the theory, for notational brevity, however, we view $\kappa > 0$ as the free parameter of the model.

The expectation value of the renormalized stress-energy tensor $\langle T^{\text{ren}}_{\mu\nu} \rangle_\omega$ is obtained by subtracting the Hadamard parametrix $H(x,y)$ from the two point function $\omega(\phi(x)\phi(y))$ of the quantum fields, applying a certain partial differential operator to $\omega(\phi(x)\phi(y)) - H(x,y)$ and performing the point splitting limit $y \to x$, see [8,32]. If $\omega(\phi(x)\phi(y)) - H(x,y)$ is infinitely often differentiable, the state $\omega(\cdot)$ is a so-called Hadamard state [16,38]. The Hadarmard parametrix is given by the asymptotic expansion of the singular part of $\omega(\cdot)$ in powers of the Synge wold function $\sigma(x,y)$ and

$$H(x,y) = \lim_{\varepsilon \to +0} \frac{1}{8\pi^2} \left(\frac{\Delta(x,y)^{\frac{1}{2}}}{\sigma(x,y) + i\varepsilon(t(x) - t(y))} + \log\left(\frac{\sigma(x,y)}{\lambda^2}\right) \sum_{j=0}^{n} \nu_j(x,y)\, \sigma(x,y)^j \right), \quad (3)$$

where t is a time function, $\Delta(x,y)$ is the van Vleck-Morette determinant and $\sigma(x,y)$, for x, y in a geodesically convex neighborhood, is the Synge world function [16,42]. The coefficient functions $\nu_j(x,y)$ are obtained recursively by the requirement that the Hadamard parametrix (truncated to order n) should fulfill the Klein-Gordon Equation (2) (up to powers $\sigma^{n+1}(x,y)$) [16,32].

In the following we restrict to flat cosmological space-times $I \times \mathbb{R}^3$, where $I \subseteq \mathbb{R}$ is a time interval and $\mathbb{R}^3$ ist the Cauchy surface. Further, the metric is given by

$$g = -dt^2 + a(t)^2 d\vec{x}^2. \quad (4)$$

Here, $t = t(x)$ is the cosmological time and $a(t)$ is the scale factor. We apply the convention that $t = t_0 = 0$ and $a(t_0) = 1$ stand for the present state of the universe. An alternative way to parametrize time is conformal time, which can be derived from the scale factor $a(t)$ via $\tau(t) = \int_{t_0}^{t} \frac{dt}{a(t)}$. Since $d\tau(t) = \frac{dt}{a(t)}$, we see that $-dt^2 + a(t)^2 d\vec{x}^2 = a^2(\tau)(-d\tau^2 + d\vec{x}^2)$, from which we instantly derive the conformal equivalence of the metric of the cosmological space-time with flat spatial section with the Minkowski metric. Here we use the (slightly misleading) convention $a(\tau)$ for the scale factor $a(t)$ at conformal time $\tau = \tau(t)$.

To study the dynamics of the SCE in the cosmological context, we wish to cast (1) in an initial value form. As described in our previous work [18], this can be achieved via the following procedure:

(i) We consider fixed time fields and momenta $\varphi(\tau, \vec{x}) = a(\tau)\phi(\tau, \vec{x})$, $\pi(\tau, \vec{x}) = \partial_\tau \varphi(\tau, \vec{x})$ and a quasi free state ω evaluated on these fields

$$\mathcal{G}(\tau, r) = \begin{pmatrix} \mathcal{G}_{\varphi\varphi}(\tau, r) \\ \mathcal{G}_{(\varphi\pi)}(\tau, r) \\ \mathcal{G}_{\pi\pi}(\tau, r) \end{pmatrix} = \lim_{\tau' \to \tau} \begin{pmatrix} \omega(\varphi(\tau, \vec{x})\varphi(\tau, \vec{y})) \\ \frac{1}{2}\omega(\varphi(\tau, \vec{x})\pi(\tau, \vec{y}) + \pi(\tau, \vec{x})\varphi(\tau, \vec{y})) \\ \omega(\pi(\tau, \vec{x})\pi(\tau, \vec{y})) \end{pmatrix} \quad (5)$$

Here it is assumed, that the state $\omega(\cdot)$ is homogeneous on fixed time fields and isotropic on the flat time sections, i.e. does only depend on $r = |\vec{x} - \vec{y}|$. Also note that only the symmetric part of the two point function enters (5), as the anti symmetric part is fixed by the CCR.

(ii) We rewrite the dynamics of the field (2) in conformal time as a dynamical equation for $\mathcal{G}(\tau, r)$ and obtain

$$\partial_\tau \mathcal{G}(\tau, r) = \begin{pmatrix} 0 & 2 & 0 \\ \Delta_r - V & 0 & 1 \\ 0 & 2(\Delta_r - V) & 0 \end{pmatrix} \mathcal{G}(\tau, r) \quad (6)$$

with $V = (6\xi - 1)\frac{a''}{a} + a^2 m^2$ and $\Delta_r = r^{-2}\partial_r r^2 \partial_r$.

(iii) Considering the corresponding fixed time formulation for $r = |\vec{x} - \vec{y}|$ at conformal time τ

$$\begin{aligned}\tilde{\mathcal{H}}(\tau, r) &= \begin{pmatrix} \tilde{\mathcal{H}}_{\varphi\phi}(\tau, r) \\ \tilde{\mathcal{H}}_{(\varphi\pi)}(\tau, r) \\ \tilde{\mathcal{H}}_{\pi\pi}(\tau, r) \end{pmatrix} \\ &= \begin{pmatrix} a(\tau)^2 H_n((\tau, \vec{x}), (\tau, \vec{y})), \\ \frac{1}{2}\left(\partial_\tau a(\tau) a(\tau') H_n((\tau, \vec{x}), (\tau', \vec{y})) + \partial_{\tau'} a(\tau) a(\tau') H_n((\tau, \vec{x}), (\tau', \vec{y}))\right)_{\tau'=\tau} \\ \left(\partial_\tau \partial_{\tau'} a(\tau) a(\tau') H_n((\tau, \vec{x}), (\tau', \vec{y}))\right)_{\tau'=\tau} \end{pmatrix}\end{aligned} \tag{7}$$

of the Hadamard parametrix (3), we obtain $\langle T^{\mathrm{ren}}_{\mu\nu} \rangle$, evaluated at conformal time, by applying a partial differential operator $\mathcal{T}_{\mu\nu}$ to $\mathcal{G} - \tilde{\mathcal{H}}$. After restricting to the diagonal, this yields a $\mathbb{R}^{4\times 4}$ valued tensor function. Restriction to the diagonal $\vec{x} = \vec{y}$ or $r = 0$ is denoted by [.]. In addition, terms that express renormalization freedom occur. Given that off-diagonal terms of the stress-energy tensor vanish for flat cosmological space-time, we can express the renormalized stress-energy tensor via its energy component $\langle T^{\mathrm{ren}}_{00} \rangle$ and trace $\langle T^{\mathrm{ren}} \rangle = g^{\mu\nu} \langle T^{\mathrm{ren}}_{\mu\nu} \rangle$, see [18]. Therewith,

$$\begin{aligned}\langle T^{\mathrm{ren}} \rangle = \big((6\xi - 1)(\xi R + m^2) - m^2\big) \frac{1}{a^2} [\mathcal{G}_{\varphi\varphi} - \tilde{\mathcal{H}}_{\varphi\varphi}] - \frac{6\xi - 1}{a^4} \big([\Delta_r (\mathcal{G}_{\varphi\varphi} - \tilde{\mathcal{H}}_{\varphi\varphi})] \\ + \frac{1}{a^2} [\mathcal{G}_{\pi\pi} - \tilde{\mathcal{H}}_{\pi\pi}] + \frac{a'^2}{a^4} [\mathcal{G}_{\varphi\varphi} - \tilde{\mathcal{H}}_{\varphi\varphi}] - 2\frac{a'}{a^3} [\mathcal{G}_{(\varphi\pi)} - \tilde{\mathcal{H}}_{(\varphi\pi)}]\big) \\ - \frac{9\xi - 2}{2\pi^2} [v_1] + 4c_1 m^4 - c_2 m^2 R - (6c_3 + 2c_4) \Box R,\end{aligned} \tag{8}$$

where $R = 6\frac{a''}{a^3}$, $\Box R = 36\frac{a'' a'^2}{a^7} - 18\frac{a''^2}{a^6} - 24\frac{a^{(3)} a'}{a^6} + 6\frac{a^{(4)}}{a^5}$ and $[v_1]$ is the conformal anomaly

$$\begin{aligned}[v_1] = \frac{m^4}{8} + \frac{1}{60}\left(\frac{a'^4}{a^8} - \frac{a'' a'^2}{a^7}\right) + \frac{(6\xi - 1) m^2}{4} \frac{a''}{a^3} + \frac{(6\xi - 1)^2}{8} \frac{a''^2}{a^6} \\ + \frac{5\xi - 1}{20}\left(6\frac{a'' a'^2}{a^7} - 3\frac{a''^2}{a^6} - 4\frac{a^{(3)} a'}{a^6} + \frac{a^{(4)}}{a^5}\right).\end{aligned} \tag{9}$$

Moreover,

$$\begin{aligned}\langle T^{\mathrm{ren}}_{00} \rangle = \frac{1}{2} [\mathcal{G}_{\pi\pi} - \tilde{\mathcal{H}}_{\pi\pi}] - \frac{1}{2a^2} [\Delta_r (\mathcal{G}_{\varphi\varphi} - \tilde{\mathcal{H}}_{\varphi\varphi})] + \frac{1}{2} m^2 [\mathcal{G}_{\varphi\varphi} - \tilde{\mathcal{H}}_{\varphi\varphi}] \\ + \xi\left(\frac{G_{00}}{a^2} [\mathcal{G}_{\varphi\varphi} - \tilde{\mathcal{H}}_{\varphi\varphi}] + 6\frac{a'}{a} [\mathcal{G}_{(\varphi\pi)} - \tilde{\mathcal{H}}_{(\varphi\pi)}] - 6\frac{a'^2}{a^2} [\mathcal{G}_{\varphi\varphi} - \tilde{\mathcal{H}}_{\varphi\varphi}]\right) \\ - \frac{a^2}{4\pi^2} [v_1] - c_1 a^2 m^4 + c_2 m^2 G_{00} + (3c_3 + c_4) J_{00}.\end{aligned} \tag{10}$$

with $G_{00} = 3\frac{a'^2}{a^2}$ and $J_{00} = -24\frac{a'' a'^2}{a^5} - 6\frac{a''^2}{a^4} + 12\frac{a^{(3)} a'}{a^4}$.

(iv) One of the problems with the Hadamard parametrix $\tilde{\mathcal{H}}(\tau, r)$ is, that it does not fulfill a well defined set of dynamic equations. We therefore introduce an auxiliary (non generally covariant) parametrix

$$\mathcal{H}_n(\tau, r) = \begin{pmatrix} 0 \\ 0 \\ \gamma_{-1}(\tau) \end{pmatrix} h_{-2}(r) + \sum_{l=0}^{n} \begin{pmatrix} \alpha_j(\tau) \\ \beta_j(\tau) \\ \gamma_j(\tau) \end{pmatrix} h_{2j}(r) \tag{11}$$

with the homogeneous distributions $h_z(r) = \frac{e^{iz\pi/2}}{2\pi^2}\frac{r^{z-2}}{\Gamma(z)}\left(\log\left(\frac{r}{\mu}\right) - \psi(z)\right)$ defined for $z \in \mathbb{C}$ via analytic continuation and depending on some parameter $\mu > 0$. Here $\psi(z)$ denotes the Digamma function. Using $\Delta_r h_j(r) = h_{j-2}(r)$, we obtain the coefficient functions $\alpha_l(\tau)$, $\beta_l(\tau)$ and $\gamma_l(\tau)$ recursively by the starting condition $\gamma_{-1} = \frac{1}{2}$, $\alpha_0 = \frac{1}{2}$ and $\beta_0 = 0$ and the equation

$$\partial_\tau \mathcal{H}_n - \begin{pmatrix} 0 & 2 & 0 \\ \Delta_r - V & 0 & 1 \\ 0 & 2(\Delta_r - V) & 0 \end{pmatrix} \mathcal{H}_n(\tau, r) = \mathcal{O}(r^{2(n-1)}). \tag{12}$$

We can then rewrite expressions like $[\mathcal{G}_\sharp - \tilde{\mathcal{H}}_{\sharp,n}]$ as $[\mathcal{G}_\sharp - \mathcal{H}_{\sharp,n}] + [\mathcal{H}_{\sharp,n} - \tilde{\mathcal{H}}_{\sharp,n}]$, $\sharp \in \{\varphi\varphi, (\varphi\pi), \pi\pi\}$, or $[\Delta_r(\mathcal{G}_\sharp - \tilde{\mathcal{H}}_{\sharp,n})]$ as $[\Delta_r(\mathcal{G}_\sharp - \mathcal{H}_{\sharp,n})] + [\Delta_r(\mathcal{H}_{\sharp,n} - \tilde{\mathcal{H}}_{\sharp,n})]$. The second term in these sums can be evaluated explicitly in terms of the scale function $a(\tau)$ and its derivatives up to order four as long as the order n is chosen larger or equal 2.

(v) We define a sequence of so-called moment functions

$$\mathcal{M}_{n,\sharp} = [\Delta_r^n(\mathcal{G}_\sharp - \mathcal{H}_{\sharp,j})],$$

$\sharp \in \{\varphi\varphi, (\varphi\pi), \pi\pi\}$, and arrange these three real-valued functions of time into $\mathbb{R}^3$-valued functions $\mathcal{M}_n = (\mathcal{M}_{n,\varphi\varphi}, \mathcal{M}_{n,(\varphi\pi)}, \mathcal{M}_{n,\pi\pi})^\top \in \mathbb{R}^3$, which are independent of j provided that $j \geq n+1$. From (6) and (12) we deduce the following recursive set of equations

$$\partial_\tau \mathcal{M}_n = A\mathcal{M}_n + B\mathcal{M}_{n+1} \quad \text{with} \quad A = \begin{pmatrix} 0 & 2 & 0 \\ -V & 0 & 1 \\ 0 & -2V & 0 \end{pmatrix} \quad \text{and} \quad B = \begin{pmatrix} 0 & 0 & 0 \\ 1 & 0 & 0 \\ 0 & 2 & 0 \end{pmatrix}. \tag{13}$$

Introducing sequences $\mathcal{M} = (\mathcal{M}_n)$ in weighted, discrete L^p-spaces $\vec{\ell}^p(w) = \mathbb{R}^3 \otimes \ell^p(w)$ with weights $w_n = w^{-n}$, $w > 1$, we obtain the dynamical system

$$\partial_\tau \mathcal{M} = (A \otimes \mathbb{1} + B \otimes \mathbb{L})\mathcal{M}, \tag{14}$$

where $\mathbb{L}$ is the left-shift operator on $\vec{\ell}^p(w)$. It has been shown that this infinite dynamical system has maximal solutions in conformal time τ for any four-times-differentiable scale function $a(\tau)$.

(vi) We consider the energy and the trace equation derived from the semiclassical Einstein equation (1)

$$-R = g^{\mu\nu}G_{\mu\nu} = \kappa\langle T^{\text{ren}}\rangle_\omega \qquad \text{and} \qquad G_{00} = \kappa\,\langle T^{\text{ren}}_{00}\rangle_\omega, \tag{15}$$

respectively. Wrapping up (i)–(v) above, one obtains

$$
\begin{aligned}
0 = &\left(-12(3c_3+c_4) - \frac{1}{480\pi^2} + \frac{6\xi-1}{48\pi^2} + \frac{(6\xi-1)^2}{16\pi^2}\log(a\lambda_0)\right) \\
&\qquad\cdot\left(\frac{a^{(4)}}{a^5} - 4\frac{a^{(3)}a'}{a^6} - 3\frac{(a'')^2}{a^6} + 6\frac{a''(a')^2}{a^7}\right) \\
&+ \frac{(6\xi-1)^2}{32\pi^2}\left(4\frac{a^{(3)}a'}{a^6} + 3\frac{(a'')^2}{a^6} - 10\frac{a''(a')^2}{a^7}\right) + \frac{1}{240\pi^2}\left(-\frac{a''(a)^2}{a^7} + \frac{(a')^4}{a^8}\right) \\
&+ \left(\frac{6}{\kappa} + m^2\Big(-6c_2 + \frac{1}{48\pi^2} + \frac{6\xi-1}{8\pi^2}\big(1+\log(a\lambda_0)\big)\Big)\right)\frac{a''}{a^3} \\
&+ \frac{(6\xi-1)m^2}{16\pi^2}\frac{(a')^2}{a^4} + m^4\left(4c_1 + \frac{1}{32\pi^2} + \frac{1}{8\pi^2}\log(a\lambda_0)\right) \\
&- \frac{m^2}{a^2}m_{\varphi\varphi,0} + (6\xi-1)\left(\Big(6\xi\frac{a''}{a^5} - \frac{(a')^2}{a^6} + \frac{m^2}{a^2}\Big)m_{\varphi\varphi,0}\right. \\
&\qquad\left. + 2\frac{a'}{a^5}m_{(\varphi\pi),0} - \frac{1}{a^4}\big(m_{\pi\pi,0} + m_{\varphi\varphi,1}\big)\right),
\end{aligned}
\tag{16}
$$

for the trace equation and

$$
\begin{aligned}
0 = &\left(6(3c_3+c_4) + \frac{1}{960\pi^2} - \frac{6\xi-1}{96\pi^2} - \frac{(6\xi-1)^2}{32\pi^2}\log(a\lambda_0)\right) \\
&\qquad\cdot\left(2\frac{a^{(3)}a'}{a^4} - \frac{(a'')^2}{a^4} - 4\frac{a''(a')^2}{a^5}\right) \\
&- \frac{(6\xi-1)^2}{16\pi^2}\frac{a''(a')^2}{a^5} + \frac{1}{960\pi^2}\frac{(a')^4}{a^6} - m^4\left(c_1 + \frac{1}{32\pi^2}\log(a\lambda_0)\right)a^2 \\
&+ \left(-\frac{3}{\kappa} + m^2\Big(3c_2 - \frac{1}{96\pi^2} - \frac{6\xi-1}{16\pi^2}\big(1+\log(a\lambda_0)\big)\Big)\right)\frac{(a')^2}{a^2} \\
&+ \frac{m^2}{2}m_{\varphi\varphi,0} + (6\xi-1)\left(-\frac{(a')^2}{2a^4}m_{\varphi\varphi,0} + \frac{a'}{a^3}m_{(\varphi\pi),0}\right) \\
&\qquad + \frac{1}{2a^2}\big(m_{\pi\pi,0} - m_{\varphi\varphi,1}\big)
\end{aligned}
\tag{17}
$$

for the energy constraint, see [18] for the details of the calculation. As a side remark of importance in later sections, note that the respective first lines of (16) and (17) consist only of contributions from the quantum theory of our field.

While the (infinite dimensional) dynamical system from (14) and (16) is well posed for any set of initial conditions $(a, a^{(1)}, a^{(2)}, a^{(3)})^\top \in \mathbb{R}^3$ and $\mathcal{m} \in \vec{\ell}^p(w)$, it is, however, not clear whether there exists a Hadamard state ω for a given set of moments $\mathcal{m}$. Let us therefore shortly comment on physical initial conditions from the 'tow-in' technique as described in [18] that guarantees the existence of physical solutions for at least a subset of moments. To this purpose, a Hadamard state and the corresponding tower of moments are prepared on some simple space-time, e.g. Minkowski space-time. Then, after a short waiting time, the space-time is deformed by an auxiliary dynamical equation that 'tows' the vector of initial conditions $(a(\tau), \dots, a^{(3)}(\tau))^\top$ to some desired vector of initial conditions $(a_0, \dots, a_3)^\top \in \mathbb{R}^4$. Both, the Hadamard state and the tower of moments propagate forward accordingly. After the tow-in phase, an interpolation phase follows where the auxilary dynamics of $(a(\tau), \dots, a^{(3)}(\tau))^\top$ and $\mathcal{m}(\tau)$ is quickly interpolated to the dynamics of the SCE given by (12) and (16). The system thereafter follows this dynamic.

It can be shown that this can be done in a way that (a) the energy constraint (17) and thereby the full SCE is fulfilled and (b) the initial conditions with respect to the dynamics $a(t)$ lie in an ε-neighbourhood to $(a_0, \dots, a_{(3)})^\top$ for $\varepsilon > 0$ arbitrary. For the details, we refer to [18, Thm. 5.11].

As the last statement of this preparatory section, we present the tower of moments for the Minkowski state with scale factor $a(\tau) = 1$. As computed in [18, (4.8)], the moments $\mathcal{m}$ in this case are given by

$$\begin{aligned} \mathcal{m}_{\varphi\varphi,n} &= \frac{1}{2\pi^2}\big(\tfrac{1}{2}m\big)^{2n+2}\Big(\log(\tfrac{1}{2}m\mu) + \psi(2n+2) - \tfrac{1}{2}\big(\psi(n+1)+\psi(n+2)\big)\Big)\binom{2n+1}{n+1}, \\ \mathcal{m}_{(\varphi\pi),n} &= 0, \\ \mathcal{m}_{\pi\pi,n} &= \frac{1}{\pi^2}\big(\tfrac{1}{2}m\big)^{2n+4}\Big(\log(\tfrac{1}{2}m\mu) + \psi(2n+2) - \tfrac{1}{2}\big(\psi(n+1)+\psi(n+3)\big)\Big)\frac{(2n+1)!}{n!(n+2)!}. \end{aligned} \tag{18}$$

It has been shown that $\mathcal{m} \in \vec{\ell}^p(w)$ for sufficiently large weights w.

3 The cSCE with zero mass and Minkowski-vacuum-like states as a dynamical system

Two observations in the dynamics of the moments in (14) and the formula for the moments of the Minkowski vacuum state in (18) are remarkable: At first, (14) is a linear homogeneous differential equation. At second, the moments for the Minkowski vacuum state vanish for $m = 0$, i.e. $\mathcal{m} = 0$ is fulfilled at the initial point of the 'tow-in' process and hence $\mathcal{m}(\tau) = 0$ holds on the entire cosmological space-time with expansion history $a(\tau)$ that partially consists of the tow-in phase and partially of the SCE phase. Hence, the quantum state completely decouples from the dynamics of the space-time. In this case, all terms in (16) and (17) that are proportional to m^2, m^4 and $\mathcal{m}$ are eliminated which largely simplifies our equations. Additional justification that this procedure actually results in physical solutions is given in Theorem 1 below. Finally, one obtains a fourth-order ODE for the scale factor $a(\tau)$ together with a third-order constraint.

Furthermore, since we are interested in cosmology including solutions with a Big Bang, we re-express the dynamic equations for $a(\tau)$ given in conformal time τ in cosmological time t. This is done in order to deal with Big Bang-solutions, as in some cases a Big Bang-event $a(t) = 0$ is shifted to conformal time $\tau = -\infty$, see also SubSection 5.3. Substituting $\frac{d}{d\tau} = a(t)\frac{d}{dt}$ the trace equation reads[1]

$$\begin{aligned} 0 = (k_2 \log(\lambda_0\, a) - k_1)\left(\frac{a^{(4)}}{a} + 3\frac{\dot{a}a^{(3)}}{a^2} + \frac{\ddot{a}^2}{a^2} - 5\frac{\dot{a}^2\ddot{a}}{a^3}\right) \\ + \frac{k_2}{2}\left(4\frac{\dot{a}a^{(3)}}{a^2} + 3\frac{\ddot{a}^2}{a^2} + 12\frac{\dot{a}^2\ddot{a}}{a^3} - 3\frac{\dot{a}^4}{a^4}\right) - k_3\frac{\dot{a}^2\ddot{a}}{a^3} + k_4\left(\frac{\dot{a}^2}{a^2} + \frac{\ddot{a}}{a}\right) \end{aligned} \tag{19}$$

where we use the dot as a symbol of derivatives w.r.t. cosmological time and for the ease of

[1] Here we employ the convention that an expression $a^{(k)}$ in an equation with dot-derivatives denotes the k-th derivative w.r.t. cosmological time whereas in an equation with prime derivatives the same expression stands tor a k-th conformal derivative. The same convention applies to initial conditions $(a_0, \dots, a_3)$.

notation we introduced

$$\begin{aligned} k_1 &= 12(3c_3 + c4) + \frac{1}{480\pi^2} - \frac{6\xi - 1}{48\pi^2}, \\ k_2 &= \frac{(6\xi-1)^2}{16\pi^2} \geq 0, \qquad k_3 = \frac{1}{240\pi^2} > 0, \qquad k_4 = \frac{6}{\kappa} > 0. \end{aligned} \tag{20}$$

The parameters k_1, k_2, k_3 are dimensionless, but a numerical value of k_4 depends on the chosen unit system. Moreover, as it has been remarked before, k_1 consists only of quantum contributions. The energy constraint in the present setting reads

$$\begin{aligned} 0 = &- (k_2 \log(\lambda_0\, a) - k_1) \left(\dot{a} a^{(3)} - \frac{1}{2}\ddot{a}^2 + \frac{\dot{a}^2 \ddot{a}}{a} - \frac{3}{2}\frac{\dot{a}^4}{a^2} \right) \\ &- k_2 \left(\frac{\dot{a}^2\ddot{a}}{a} + \frac{\dot{a}^4}{a^2} \right) + \frac{k_3}{4}\frac{\dot{a}^4}{a^2} - \frac{k_4}{2}\dot{a}^2. \end{aligned} \tag{21}$$

Let us next reconsider the 'tow-in' procedure for the proof of the existence of a physical Hadamard state which corresponds to some dynamics of moments $\mathcal{M}(\tau)$ for the special case that we start the tow-in process with $\mathcal{M} = 0$ and hence obtain $\mathcal{M}(\tau) = 0$. In this special case we can refine the results of [18] on the existence of physically meaningful solutions to the cSCE in an arbitrarily small neighborhood of the initial conditions $(a_0, \ldots, a_3)^\top$ for $a(t)$ at $t = 0$ and its first to third derivatives. In the present context we modify the tow-in argument and prove that any set of initial conditions $(a_0, \ldots, a_3)^\top$ with $k_2 \log(\lambda_0 a_0) - k_1 \neq 0$ can be matched *exactly*:

Theorem 1. *Let $(a_0, \ldots, a_3)^\top \in (0, \infty) \times \mathbb{R}^3$ be initial values for $a(t)$ at cosmological time $t = 0$ such that $(k_2 \log(\lambda_0 a_0) - k_1) \neq 0$. Then*

(i) *There exists $a(t)$, a unique solution to the ODE* (19) *on some interval of time $(t_\mathrm{i}, t_\mathrm{f})$, $t_\mathrm{i} \in [-\infty, 0)$, $t_\mathrm{f} \in (0, \infty]$, such that $a(t)$ fulfills* (19) *with the given initial conditions;*

(ii) *If the initial conditions fulfill the energy constraint* (21) *at $t = 0$, then* (21) *is fulfilled for all times;*

(iii) *There exists a Hadamard state on the cosmological space-time defined by $a(t)$, $t \in (t_\mathrm{i}, t_\mathrm{f})$ for the massless Klein-Gordon field with associated tower of moments fulfilling $\mathcal{M}(t) = 0$.*

Hence, any cosmological space-time definded by $a(t)$ for $t \in (t_\mathrm{i}, t_\mathrm{f})$ as described in (i) *and* (ii) *is a solution to the cSCE for Hadamard state as in* (iii).

Proof. Note that by the assumption $(k_2 \log(\lambda_0 a_0) - k_1) \neq 0$ equation (19) can be brought to the form

$$a^{(4)} = f(a, \dot{a}, \ddot{a}, a^{(3)})$$

where $f(\cdot)$ is locally Lipschitz except for $a = 0$ and $(k_2 \log(\lambda_0 a(t)) - k_1) = 0$. Therefore assertion (i) follows from standard theory of ODE, see e.g. [1].

Since the energy equation is a constant of motion for the trace equation, statement (ii), is well known, see, e.g. eq. (22) below.

To prove (iii) we modify the 'tow-in' argument from Section 2 in the following way: let $(t_\mathrm{i}, t_\mathrm{f})$ be an interval containing $t = 0$ such that the solution $a(t)$ from (i) is given.

Consider the switching function $\chi \in C^\infty(\mathbb{R}, [0, 1])$ with the property $\chi(t) = 0$ for $t < \frac{3}{4}t_\mathrm{i}$ and $\chi(t) = 1$ for $t > \frac{1}{4}t_\mathrm{i}$. Moreover, consider the cosmological space-time defined by the smooth scale factor

$$a_\mathrm{tow}(t) = \chi(t) a(t) + (1 - \chi(t)),$$

which is Minkowski for $t \leq \frac{3}{4}t_\mathrm{i}$.

We can thus consider ω_vac, the Minkowski vacuum state for the massless free field for values $t < \frac{3}{4}t_\mathrm{f}$, which is propagated forward to a state ω_tow on the entire (globally hyperbolic) space-time defined by a_tow via the massless Klein-Gordon dynamics. As the Minkowski vacuum state ω_vac is Hadamard and $a_\mathrm{tow}(t)$ is smooth, so is the propagated state ω_tow [18].

Furthermore, the tower of moments $\mathcal{m}_\mathrm{vac}(t)$ associated to ω_vac for $t < \frac{3}{4}t_\mathrm{i}$ by (18) fulfills $\mathcal{m}_\mathrm{vac}(t) = 0$ and therefore by (14) the tower of moments associated with ω_tow fulfills $\mathcal{m}_\mathrm{tow}(t) = 0$ also for $t \in (t_\mathrm{i}, t_\mathrm{f})$. By this circumstance, the cSCE is fulfilled on $(\frac{1}{4}t_\mathrm{i}, t_\mathrm{f})$. Lastly, if the state is defined on this interval of time, it can be propagated backwards to a state ω on the (also globally hyperbolic) space-time defined by $a(t)$, $t \in (t_\mathrm{i}, t_\mathrm{f})$ which, for the same reasons as above, results is a Hadamard state on this cosmological space-time. Here again the associated tower of moments fulfills $\mathcal{m}(t) = 0$, for $t \in (t_\mathrm{i}, t_\mathrm{f})$ as $\mathcal{m}(t) = \mathcal{m}_\mathrm{tow}(t) = 0$ for $t > \frac{1}{4}t_\mathrm{i}$ and (14). Thus ω, $a(t)$ and $\mathcal{m}(t)$ fulfill the cSCE. This proves the third assertion. □

Let us shortly compare Theorem 1 to the well-known decoupling result for massless conformal fields by Starobinski [40]. In the case of conformal coupling, Starobinski's result is more general, as *every* state decouples from the cSCE, up to the conformal anomaly term. Our result is resticted to a special class of towed-in massless Minkowski vacuum states, exclusively. On the other hand, our result is more general as conformal coupling $\xi = \frac{1}{6}$ is not required.

A last remark in the present section is on the role of the regularization parameter λ_0. Since it is only used to construct the auxiliary parametrices, it does not bear any physical meaning. Nevertheless, different values for λ_0 lead to different solutions $a(t)$. Note, however, that ω_vac has to be towed in via the λ_0 dependent space-time defined by $a_\mathrm{tow}(t)$ and therefore also the state ω_tow on $(\frac{3}{4}t_\mathrm{i}, t_\mathrm{f})$ implicitly depends on λ_0.

4 General discussion on the decoupled cSCE

One can easily see that the trace equation (19), with the energy equation (21) regarded as an algebraic constraint (particularly, on the initial values), and the energy equation, regarded as an ODE in its own right, are equivalent under the assumption $\dot{a} \neq 0$. This observation can be traced back to a property of the Einstein tensor's components in FLRW space-time, namely that

$$\frac{\mathrm{d}}{\mathrm{d}t}\big(a^2\, G_{00}\big) + 2a\dot{a}G_{00} = -a\dot{a}\; g^{\mu\nu}G_{\mu\nu}, \tag{22}$$

and thus, imposed by the SCE (1), the analog equation holds for $\langle T^\mathrm{ren}_{\mu\nu}\rangle_\omega$ as well. However, due to the latter restriction $\dot{a} = 0$ and in order to avoid numerical difficulties close to the $\dot{a} = 0$-regime, we prefer to work with the trace equation (19). By the aforementioned equivalence we then conclude that choosing suitable initial conditions to fulfill (21) results in solutions which fulfill (21) for all times.

Some exact solutions can be found by the ansatz $a(t) = \exp(Ht)$. Inserting it into either the trace equation or the energy constraint, we obtain a fourth order polynomial equation for H solved by

$$H = 0 \qquad \text{or by} \qquad H = \pm H^\mathrm{dS} := \pm\sqrt{\tfrac{2k_4}{k_3 - 8k_2}}. \tag{23}$$

Obviously, $H = 0$ stands for the Minkowski solution while $\pm H^\mathrm{dS}$ are expanding/shrinking de Sitter solutions with constant Hubble parameter $H = \frac{a'(t)}{a(t)}$. Note that H^dS is a real number if and only if $k_2 < \frac{k_3}{8}$, or equivalently, $|\xi - \frac{1}{6}| < \sqrt{1/4320}$. The symmetric occurrence of expanding and shrinking de Sitter solutions is a consequence of the time reflection invariance $t \to -t$ of

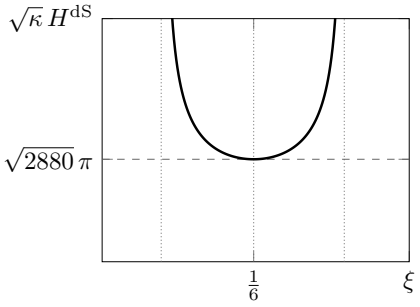

Figure 1: The (constant) Hubble rate H^{dS} of the de Sitter solutions defined in (23), shown as a function of ξ. The vertical axis is rescaled by $\sqrt{\kappa}$ as H^{dS} is proportional to this value and the graphic depends on no other parameter. The dotted vertical lines show the distinguished values $\xi \in \{\frac{1}{6}, \frac{1}{6} \pm \sqrt{1/4320}\}$. We see the analog graphic to the massless, $\Lambda = 0$-case of [17].

the cSCE which can be easily read off from the decoupled equations and which will be furtherly exploited below.

We note that the de Sitter solutions found here are not necessarily identical to those discussed in [25], as the 'tow-in' states we consider here are constructed very differently from the Bunch-Davies state for the massless field. A complete list of de Sitter solutions based on Bunch-Davis states (massless and massive) is given in [17].

Remark 2. *Note the similarity of Figure* 1 *with a particular graphic in* [17]*, namely the one which shows the de Sitter Hubble rate H as a function of ξ in the massless $\Lambda = 0$-case. Despite that in* [17] *a different state was chosen, the polynomial equation to be solved for H is very similar. Particularly, the same analysis as in* [17] *may be performed for our 'tow-in'-states, also with $\Lambda \neq 0$, and we would analogously observe a quantum branch and a (semi-) classical branch of de Sitter solutions for $\Lambda > 0$.*

The problem further simplifies if $\xi = \frac{1}{6}$ and $3c_3 + c_4 = -\frac{1}{5760\pi^2}$, or $k_1 = k_2 = 0$, respectively, as e.g. considered by Starobinski [40]. In this setting it suffices to take into account the energy constraint. The latter then reads as

$$0 = \frac{k_3}{4}\,\frac{\dot{a}^4}{a^2} - \frac{k_4}{2}\dot{a}^2 \tag{24}$$

and is solved by either $\dot{a}(t) = 0$ or by $\dot{a}(t) = H\,a(t)$ with $H = \pm\sqrt{\frac{2k_4}{k_3}} = \pm H^{\mathrm{dS}}$. In this scenario, the Minkowski and de Sitter solutions thus are the only ones.

In the general case, we solve the decoupled cSCE numerically. This requires the specification of initial conditions and insight into the dependency on the parameters $k_1, \ldots, k_4$. Let us start with a discussion of the initial conditions, a parameter study will be done in the subsequent section.

At first, we note that the set of solutions of both our equations are invariant under transformations of the form

$$a(t) \;\mapsto\; \beta_1\, a(\beta_2\, t + \beta_3) \tag{25}$$

($\beta_1, \beta_2, \beta_3 \in \mathbb{R},\ \beta_2 \neq 0$), at least with simultaneous redefinitions $k_4 \mapsto \beta_2^2\, k_4$ and $k_1 \mapsto k_1 - k_2 \log(\beta_1)$. Particularly, for a full study of initial conditions and parameters we can fix our initial time to be zero at the present time and our initial value of the scale factor of the present universe to $a(0) = a_0 = 1$.

A physical initial value for $\dot{a}(t)$ is the present day Hubble constant H_0, which is 2.2×10^{-18} sec^{-1} in SI-units or 1.19×10^{-61} in Planck units [34]. However, by the invariance of our equations under (25) this value is rather arbitrary and should be viewed as a physically realistic choice.

For the initial value of $\ddot{a}$ we introduce the deceleration parameter

$$q_0 = -\frac{a\ddot{a}}{\dot{a}^2}\,, \tag{26}$$

which is an invariant quantity under the transformations (25). For any given pair $a(0)$ and $\dot{a}(0) \neq 0$ the deceleration parameter q sets the initial conditions for $\ddot{a}(0)$. In our numerical studies we mostly use $q_0 = -0.538$ from ΛCDM cosmology [34] (cf. also the discussion below). However, we emphasize that we also view this value merely as a physically realistic choice.

Finally, as mentioned before, for a given triple $(a(0), \dot{a}(0), \ddot{a}(0))^\top = (a_0, a_1, a_2)^\top$ we solve (21) for a consistent value of $a_3 = a^{(3)}(0)$. Unless $\dot{a}(0) = 0$ the solution for a_3 is unique.

As, in the end, we want to compare our equation's solutions to the ΛCDM model, we want to shortly (and partially) discuss its derivation. Mainly, this model is based on a certain observation on the Friedmann equations. These, in turn, are derived from the Einstein equation $G_{\mu\nu} = 8\pi G\, T_{\mu\nu}$ with the assumption of a cosmological metric (4). Moreover, one imposes the stress-energy tensor to be of the same homogeneity and isotropy type, a so-called perfect-fluid stress-energy tensor

$$(T^\mu{}_\nu) = \mathrm{diag}(-\varrho, p, p, p) \tag{27}$$

with functions ϱ and p, called the energy density and the pressure, respectively. The resulting equations bear special solutions, namely by imposing the state equation $p = \gamma \cdot \varrho$ we obtain

∘	the radiation solution	$a(t) \propto (t - t_{\mathrm{BB}})^{1/2}$	with $\gamma = \frac{1}{3}$,	
∘	the dust solution	$a(t) \propto (t - t_{\mathrm{BB}})^{2/3}$	with $\gamma = 0$	and the
∘	the Dark Energy solution	$a(t) \propto \exp(Ht)$	with $\gamma = -1$	

(28)

(for some Big Bang times t_{BB} and some Hubble rate H). For these three classes of solutions we, moreover, observe that $\varrho \propto \frac{1}{a^4}$, $\varrho \propto \frac{1}{a^3}$ and $\varrho = \mathrm{const.}$, respectively, and the ΛCDM model is, finally, obtained by assuming ϱ to be a superposition of these three types of energy content. Formally, we make the ansatz $\varrho = \varrho_0\big(\frac{\Omega_{\mathrm{rad}}}{a^4} + \frac{\Omega_{\mathrm{dust}}}{a^3} + \Omega_{\mathrm{DE}}\big)$ and obtain the equation

$$H^2 = H_0^2\Big(\frac{\Omega_{\mathrm{rad}}}{a^4} + \frac{\Omega_{\mathrm{dust}}}{a^3} + \Omega_{\mathrm{DE}}\Big) \tag{29}$$

as a cosmological model, where $H = H(t) = \frac{\dot{a}(t)}{a(t)}$ is the Hubble rate at time t. Hereby ϱ_0, H_0, Ω_{rad}, Ω_{dust} and Ω_{DE} are some (not necessarily independent) parameters of the model, in particular, the latter three fulfill $\Omega_{\mathrm{rad}} + \Omega_{\mathrm{dust}} + \Omega_{\mathrm{DE}} = 1$. Whenever we speak of 'standard values' for these parameters we mean the values

$$\Omega_{\mathrm{rad}} = 5.38 \cdot 10^{-5}, \quad \Omega_{\mathrm{dust}} = 0.315, \quad \Omega_{\mathrm{DE}} = 0.685$$

and H_0 as above, taken from [34]. Note that these values are subject to measurement uncertainty. We denote the resulting solution by $a_{\Lambda\mathrm{CDM}}$.

However, motivated by the ΛCDM model's derivation we want to introduce another quantity which will frequently find use in our later discussions. Define

$$\Gamma[\,a\,](t) := -\frac{1}{3}\Big(2\frac{a(t)\,\ddot{a}(t)}{\dot{a}(t)^2} + 1\Big) = \tfrac{2}{3}\,q[\,a\,](t) - \tfrac{1}{3},$$

for sufficiently nice (particularly with $\dot{a} \neq 0$) scale factors $a : I \to (0, \infty)$ on some interval I. In the last equality we used the notation $q[\,a\,] = -\frac{a\ddot{a}}{\dot{a}^2}$, obviously inspired by (26). Moreover, we note that using the above parameter values for Ω_{rad}, Ω_{dust} and Ω_{DE} as well as the ΛCDM

equation (29), one can compute $q[a_{\Lambda\mathrm{CDM}}](0) = -0.538$, that is, the value we have introduced above.

Note that Γ has an interesting physical content. For the solutions of the Friedmann equations mentioned above, Γ reproduces the corresponding values of γ and, conversely, if we read the conditions $\Gamma[\,a\,] \in \{-1, 0, \frac{1}{3}\}$ as ODE's in their own right, we reproduce the corresponding Friedmann solutions form (28) and only these. Observing the existence of two more solutions to the ΛCDM model, namely

$$a(t) \propto \sinh(\beta t)^{1/2} \qquad \text{and} \qquad a(t) \propto \sinh(\beta t)^{2/3}$$

for $\Omega_{\mathrm{dust}} = 0$ and for $\Omega_{\mathrm{rad}} = 0$, respectively, we observe that these solutions interpolate between a radiation- or dust-like behavior at early times and a Dark Energy-like behavior at late times. Γ in these cases reads as

$$\Gamma\big[\sinh(\beta t)^{1/2}\big] = \tfrac{1}{3} - \tfrac{4}{3}\tanh(\beta t)^2 \qquad \text{and} \qquad \Gamma\big[\sinh(\beta t)^{2/3}\big] = -\tanh(\beta t)^2,$$

respectively, and thus, physically spoken, Γ shows how much a given universe is radiation/dust dominated or Dark Energy dominated at a certain phase.

As a final comment on Γ, note that for any stress-energy tensor of the shape (27) the corresponding (classical or semiclassical) Einstein equation immediately implies[2] that $\Gamma = \frac{p}{\varrho}$. Particularly, also the solutions of our trace equation (19) may be assigned with an energy content of the Friedmann solutions' types, allowing a physical interpretation.

For our numerical simulations we want to exploit the invariance under (25). To avoid numerical instability, we rescale with $\beta_2 = \frac{1}{H_0}$ (and, correspondingly, redefine k_4) and end up with the initial value $\dot{a}(0) = a_1 = 1$ in the new time scale. q_0 is not affected by our rescaling and $a^{(3)}$ is still computed by the energy equation, now with k_4 in the new time scale. λ_0 is usually set to 1, as a different value may be absorbed into the renormalization freedom. We employ the standard stiff[3] equation solver `ode15s` of the MATLAB® R2020a release[4].

A typical solution with the parameters

- $\dot{a}(0) = H_0 = 2.2 \cdot 10^{-18}\frac{1}{\mathrm{s}}$
- $\ddot{a}(0)$ given by $q_0 = q_{0,\Lambda\mathrm{CDM}} = -0.538$
- $\xi = \frac{1}{12}$
- $3c_3 + c_4 = 0.5$
- $\lambda_0 = 1$
- $\kappa = 2{\cdot}10^{42}$

is shown in Figure 2. It is typical in the sense that its behavior as a function of time is generic for a certain range of parameters that has been identified manually in order to retrieve promising cosmological models. The most remarkable of these properties are an exponential late time expansion as well as a 'square-root-like zero' at early times. In other words, we indeed observe a solution which admits a Big Bang and immediately after this Big Bang the universe expands asymptotically as $a(t) \propto (t - t_{\mathrm{BB}})^{1/2}$. To underpin this notion of 'square-root-like' we have included a plot of the solution a of Figure 2 − together with its first two derivatives − in Figure 3. The horizontal axes in Figure 3 are now shifted to $t - t_{\mathrm{BB}}$ (with a numerically obtained value t_{BB}), allowing a log-log-scaling. The red dotted lines show the analog curves for a pure square-root expansion with the same Big Bang time and, particularly, how the latter fits our solution over several magnitudes. Moreover, computing the Ricci scalar curvature for the metric (4), that is $R = 6\big(\frac{\ddot{a}}{a} + \frac{\dot{a}^2}{a^2}\big)$, we find that our Big Bang is indeed a singularity in the sense that $R \to \infty$ as $t \to t_{\mathrm{BB}}$.

[2] As we defined Γ, it is nothing but the fraction of the Einstein tensor's respective diagonal entries for a FLRW metric.

[3] We are particularly interested in Big Bang solutions.

[4] A comparison to other solvers showed little to no deviation between solutions, with deviations decreasing as the solvers' accuracies were increased.

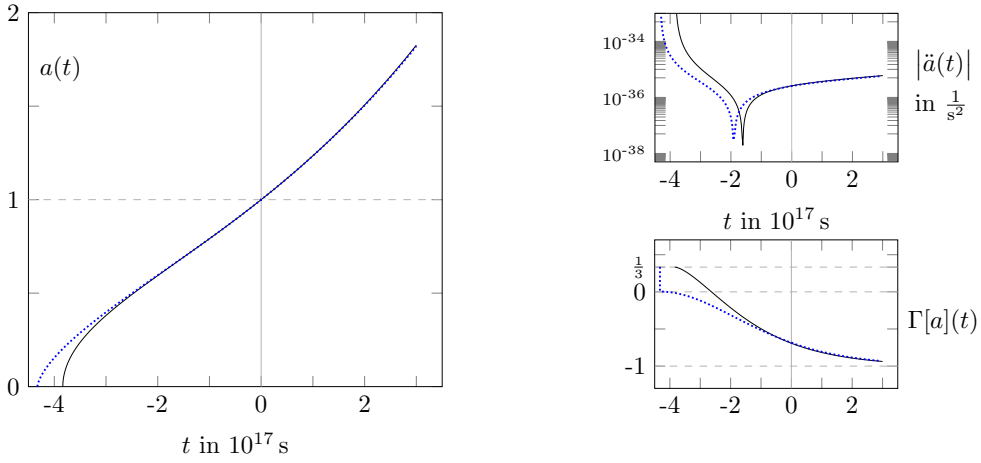

Figure 2: Solution of the cSCE (black), compared to the best fit (i.e. using numeric values from [34], cited in the text) ΛCDM model (dotted blue)

In terms of the quantity Γ, the above observations can be interpreted as a radiation dominated early phase and a Dark Energy dominated late time expansion. The former does match the physical expectation that a massless scalar field should behave like radiation, and the latter does again indicate an effect of Dark Energy, although we did not include a cosmological constant to our model. Note that one cannot easily blame a non-vanishing cosmological constant for this effect, since the influence of c_1 (that is, the renormalization constant of Λ) is ruled out by setting $m = 0$.

Remark 3. *Note that for metrics of the form* (4) *one can compute*

$$\tfrac{1}{6}\,\Box\, R = \frac{a^{(4)}}{a} + 3\frac{\dot{a}a^{(3)}}{a^2} + \frac{\ddot{a}^2}{a^2} - 5\frac{\ddot{a}\dot{a}^2}{a^3},$$

that is, the first line of (19) *is proportional to* $\Box R$*. Hence, for parameters* $\varepsilon := 3c_3 + c_4, \xi$ *and* κ *(as well as* λ_0*) such that* $k_1 \gg k_2, k_3, k_4$*, the trace equation is expected to be well approximated by*

$$\Box\, R = 0, \tag{30}$$

at least sufficiently far away from the singularity defined by $k_2 \log(\lambda_0 a) - k_1 = 0$*. Note that* (30) *is also solved by* $a(t) \propto (t - t_{\mathrm{BB}})^{1/2}$*, by* $a(t) \propto \exp(Ht)$ *and by* $a(t) \propto \sinh(t - t_{\mathrm{BB}})^{1/2}$*, which in turn solve the* Λ*CDM model for particular choices of matter.*

5 Numeric solutions of the cosmological semiclassical Einstein equation

In the present section we want to identify a few regions of interest in the parameter space of or cosmological model.

Throughout this section we will denote $\varepsilon = 3c_2 + c_3$ and usually we set $\lambda_0 = 1$. Moreover, we denote $\varepsilon_{\mathrm{crit}} = \varepsilon_{\mathrm{crit}}(\xi)R$ to be the value such that $k_1(\varepsilon, \xi)$ vanishes. Recall that varying $\dot{a}(0)$ does not influence the shape of our solutions and may be regarded as a redefinition of a time scale (while accordingly adjusting κ's units). Thus we generally omit an investigation of the dependency of our solutions on λ_0 and $\dot{a}(0)$.

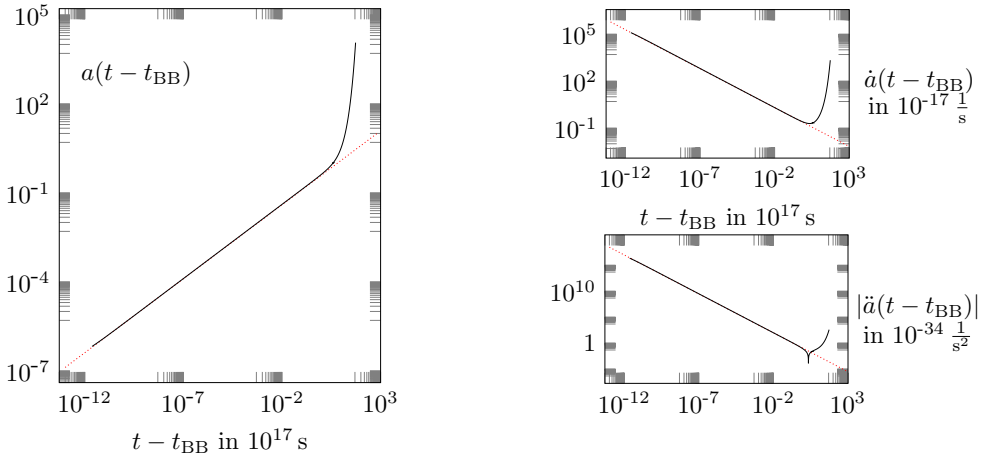

Figure 3: Double logarithmic plot of the solution in Figure 2 (black), together with the regression lines whose slopes coincide with a square-root function (dotted red)

5.1 Influence of the renormalization freedom and the curvature coupling

We start the numerical investigations with the parameter dependency of solutions of the generic type shown in Figures 2 and 3 and summarize our results in Figure 4. One can see many more numerical solution which we count to the generic class.

The choice of values of ε was made to emphasize the distinguished cases $\varepsilon = 0$ (curve (e) in Fig. 4), and $\varepsilon = -\frac{1}{5760\pi^2}$ (curve (f) in fig. 4, note that $\varepsilon_{\mathrm{crit}}(\frac{1}{6}) = -\frac{1}{5760\pi^2}$), where the renormalization freedom cancels the parameter-independent term in k_1. Both of them are continuously embedded (w.r.t. an appropriate topology) into the depicted one-parameter family of curves. A third distinguished ε-value is given by $\varepsilon = \varepsilon_{\mathrm{crit}}(\frac{1}{12}) = -\frac{1}{960\pi^2} \approx -1.05 \cdot 10^{-4}$, to be seen in between curves (g) and (h) in Figure 4. For this value we have $k_1 = 0$ as well as $a_{\mathrm{crit}} = 1$ and we cannot solve our trace equation for $a^{(4)}$ at our choice of initial values. Close to that value we observe unstable behavior. For the value of $\xi = \frac{1}{12}$, where there exists no pure de Sitter solution (cf. Figure 1), was chosen as an example for cases with the aforementioned property. Different values for ξ produce similar graphics.

Note that any solution exists until it runs into one of the singularities $a = 0$ or $a = a_{\mathrm{crit}}$. Around the aforementioned instability at $\varepsilon = \varepsilon_{\mathrm{crit}}(\frac{1}{12})$ we observe that a_{crit} approaches the value 1 and, accordingly, end up with a short interval of existence.

Remark 4. *We want to emphasize that any numerical solution we have observed running into the a_{crit}-singularity, does that with an apparently finite value of $\dot{a}$. This is not very surprising since the vector field we integrate for the solution has a pole of order one at a_{crit}. Hence a sloppy analysis suggests that a is a function whose fourth derivative has a pole of order one, implying that its third derivative has a logarithmic pole and that its second and first derivatives as well as a itself can be continuously extended to that critical point and beyond.*

Note that the immediate output of our numerical solver, which returns a and its first three derivatives, shows that $\dot{a}$ diverges in such points. Plugging the solvers output into the energy constraint's RHS, and recalling the discussion from the beginning of Section 4, however, suggest this divergence to be a numerical artifact.

The unstable behavior for $\varepsilon \to \varepsilon_{\mathrm{crit}}(\frac{1}{12}) = -\frac{1}{960\pi^2}$ can now be characterized as follows. As $\varepsilon \to \varepsilon_{\mathrm{crit}}(\xi)$ we have $a_{\mathrm{crit}} \to 1$. Hence, on the one hand, if $\varepsilon < \varepsilon_{\mathrm{crit}}(\frac{1}{12})$ we have an existence

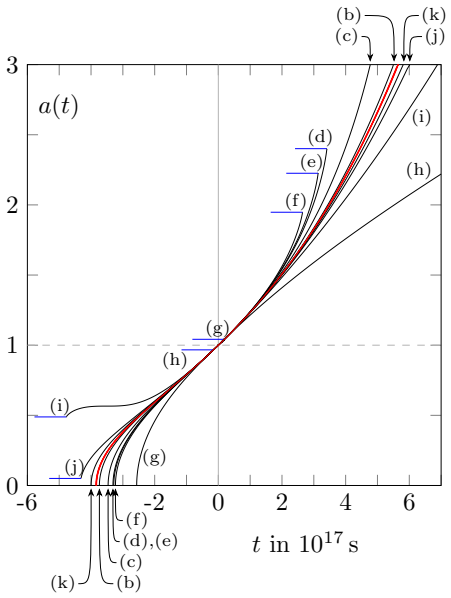

Parameters:

- $\dot{a}(0) = H_0$
- $q_0 = -0.538$
- $\kappa = 2 \cdot 10^{42}$
- $\lambda_0 = 1$
- $\xi = \frac{1}{12}$

	ε	$\exp\left(\frac{k_1}{k_2}\right)$
(a)	$\leq -10^{-2}$	≈ 0
	$\geq 10^{-2}$	$\approx \infty$
(b)	10^{-3}	4358.4
(c)	10^{-4}	4.7492
(d)	10^{-5}	2.4008
(e)	0	2.2255
(f)	$-\frac{1}{5760\pi^2}$	1.9477
(g)	-10^{-4}	1.0429
(h)	$-1.1 \cdot 10^{-4}$	0.9668
(i)	$-2 \cdot 10^{-4}$	0.4887
(j)	$-5 \cdot 10^{-4}$	0.0503
(k)	-10^{-3}	0.0011

Figure 4: Influence of the parameter $\varepsilon = 3c_3 + c_4$ shown is a family of solutions. The cases '$\leq -10^{-2}$' and '$\geq 10^{-2}$' labeled by (a) contain the values $\{-100, -1, -\frac{1}{10}, -10^{-2}\}$ and $\{10^{-2}, \frac{1}{10}, \frac{1}{2}, 100\}$, respectively, yielding a critical value for a of numerical zero or numerical infinity. All these solutions show no significant difference among each other and are covered by the red curve. The blue lines mark the respective critical value of $a_{\text{crit}} = \exp\left(\frac{k_1}{k_2}\right)$ for the other cases.

interval of $(-\eta, \infty)$ with some $\eta_\varepsilon > 0$ where

$$\eta_\varepsilon \to 0 \text{ as } \varepsilon \to \varepsilon_{\text{crit}}(\tfrac{1}{12}) \quad \text{and} \quad \eta_\varepsilon \to t_{\text{BB,eff}} \text{ as } \varepsilon \to \infty$$

with some $t_{\text{BB,eff}}$, playing the role of a Big Bang time in the limit. On the other hand, if $\varepsilon > \varepsilon_{\text{crit}}(\frac{1}{12})$ the solution exist on an interval (t_{BB}, η) for some $\eta > 0$, now with

$$\eta \to 0 \text{ as } \varepsilon \to \varepsilon_{\text{crit}}(\tfrac{1}{12}) \quad \text{and} \quad \eta \to \infty \text{ as } \varepsilon \to -\infty.$$

If we want to combine the two resulting limits for $\varepsilon \to \varepsilon_{\text{crit}}(\frac{1}{12})$, defined on the intervals $(0, t_{\text{BB}})$ and $(0, \infty)$, respectively, our numerical analysis suggests that we obtain a square-root power law expansion. This is already indicated in curves (g) and (h) in Figure 4 (or their respective branch). This behavior becomes more pronounced, if we choose values of ε even closer to $\varepsilon_{\text{crit}}(\frac{1}{12})$.

Finally,the term $k_1 \Box R$ in the trace equation, which originates in pure quantum effects, usually induces solutions with an exponential late-time expansion as remarked in Section 2.

Remark 5. *Recall R. M. Wald's classical work* [41] *where he shows that solutions to the (classical) cosmological Einstein equation with a positive cosmological constant usually (i.e. under some assumption on the stress-energy tensor) show a late time exponential expansion. Thus it is noteworthy that in our case the $k_1 \Box R$ term seemingly plays a similar role as the classical cosmological constant. Tuning the prefactor of $\Box R$ to zero we apparently restore a purely radiation dominated expansion.*

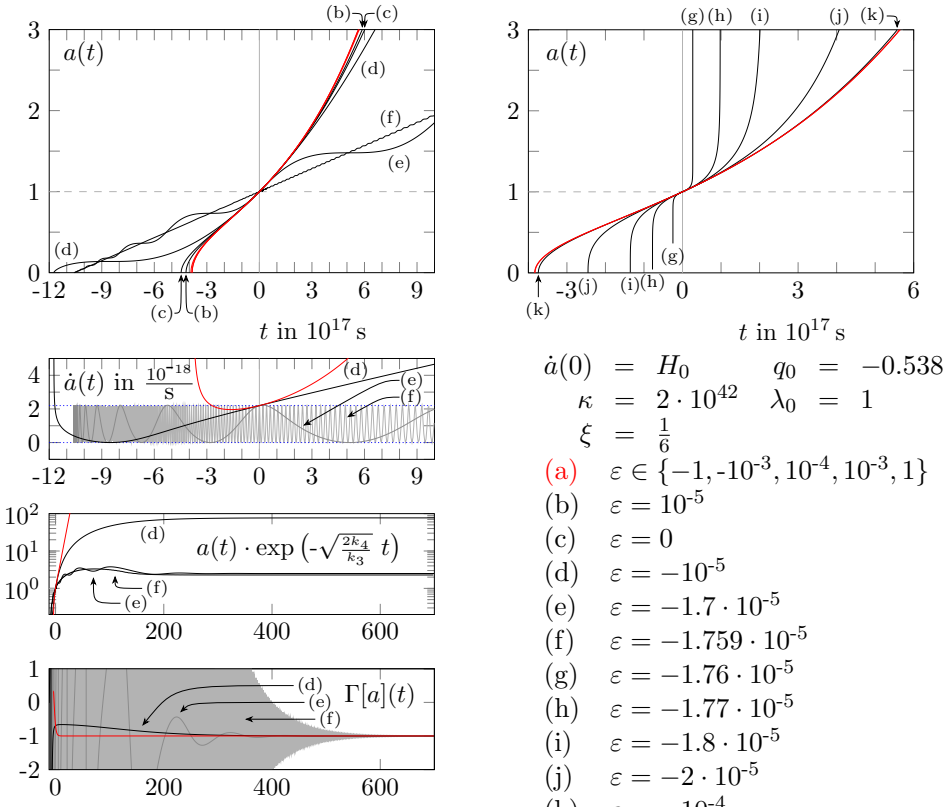

$\dot{a}(0) = H_0 \qquad q_0 = -0.538$
$\kappa = 2 \cdot 10^{42} \qquad \lambda_0 = 1$
$\xi = \frac{1}{6}$

(a) $\varepsilon \in \{-1, -10^{-3}, 10^{-4}, 10^{-3}, 1\}$
(b) $\varepsilon = 10^{-5}$
(c) $\varepsilon = 0$
(d) $\varepsilon = -10^{-5}$
(e) $\varepsilon = -1.7 \cdot 10^{-5}$
(f) $\varepsilon = -1.759 \cdot 10^{-5}$
(g) $\varepsilon = -1.76 \cdot 10^{-5}$
(h) $\varepsilon = -1.77 \cdot 10^{-5}$
(i) $\varepsilon = -1.8 \cdot 10^{-5}$
(j) $\varepsilon = -2 \cdot 10^{-5}$
(k) $\varepsilon = -10^{-4}$

Figure 5: Solutions of the trace equation with the listed parameters. Note that the critical value of renormalization constants is given by $\varepsilon_{\text{crit}} = -\frac{1}{5760\pi^2} \approx -1.75905 \cdot 10^{-5}$, in between the respective parameters of curve (f) and (g). Solutions for values above the latter are plotted on the left, for values below on the right. Just above that critical value the solutions gather an oscillatory behavior. To emphasize this the lower three graphics on the left show $\dot{a}$, a compared to our limiting de Sitter-solution and $\Gamma[\,a\,]$, respectively. The dotted blue lines in the $\dot{a}$-plot mark the interval $[0, H_0]$.

As a second part of this section, we want to discuss the influence of the curvature coupling ξ. From a physical point of view, we have the distinguished cases $\xi = 0$, called minimally coupled case, and $\xi = \frac{1}{6}$, called conformally coupled case.

As we have discussed before, in the case $\xi = \frac{1}{6}$ the trace equation simplifies significantly. Particularly we have $k_2 = 0$, which cancels many terms of the trace equation including the $\log(a)$-term. Then the influence of the $k_1 \,\Box\, R$-term is controlled by one parameter only, namely ε, and not by a possibly singular dependency on the value of a (such as our $\log(a)$-term). Particularly, we have no critical value of a. In the limit $k_1 \to 0$ or $\varepsilon \to \varepsilon_{\text{crit}}(\frac{1}{6}) = -\frac{1}{5760\pi^2}$, respectively. We are thus back in the Starobinski scenario from Section 4.

Some numerical solutions for $\xi = \frac{1}{6}$ are shown in Figure 5. Recall that in Figure 4 the behavior is different if we approached the critical value of ε from below or above, but the limiting curves appeared to be consistent. In Figure 5 in turn this is not the case anymore. As expected, for a large absolute value of ε we recover the generic solution class as before.

If we approach $\varepsilon \to -\frac{1}{5760\pi^2}$ from above we can see how an oscillating behavior fades in. Curve (i) of Figure 4 (where we also approached $k_1 \to 0$ from below) behaves similarly, but there the

solutions stop existing after a specified time due to the critical value of $a_{\text{crit}} = \exp\left(\frac{k_1}{k_2}\right) \in (0,1)$. The oscillation's frequency grows, as $\varepsilon \to -\frac{1}{5760\pi^2}$ and decays as $t \to \infty$. The amplitude in turn decays as $\varepsilon \to -\frac{1}{5760\pi^2}$ but grows as $t \to \infty$. Solutions decay in steps and the slope of these steps is bounded by the initial value $\dot{a}(0) = H_0$ from above as well as by 0 from below. This boundary interval is indicated by the blue dotted line in the $\dot{a}$-plot in Figure 5. In the limit $\varepsilon \to -\frac{1}{5760\pi^2}$, our solutions seemingly converge to a linear expansion, but this is no longer true on a larger time scale not displayed in the figure, where we find de Sitter expansion, again. This can be seen in the logarithmic plot of $a(t) \cdot \exp(-H^{\text{dS}}t)$ with $H^{\text{dS}} = \sqrt{\frac{2k_4}{k_3}}$ (i.e. H^{dS} from (23) in the case $\xi = \frac{1}{6}$, or $k_2 = 0$, resp.), cf. Figure 5. Note that all solutions for sufficiently small $k_1 > 0$ result in an exponential late-time expansion with de Sitter rate H^{dS}. The latter value can be determined by solving the limit equation

$$a^{(4)} = -\frac{k_3}{k_1}\frac{\dot{a}^2\ddot{a}}{a^2} + \frac{k_4}{k_1}\Big(\frac{\dot{a}^2}{a} + \ddot{a}\Big)$$

with a de Sitter ansatz $a(t) \propto \exp(Ht)$. This equation is obtained by solving (19) for $a^{(4)}$ and neglecting all terms which do not scale by $\frac{1}{k_1}$. The limit equation yields $H = \sqrt{\frac{2k_4}{k_1+k_3}}$,which recovers the $\xi = \frac{1}{6}$-value of H^{dS} in the limit $k_1 \to 0$.

The emergence of late time de Sitter expansion can also be observed in the $\Gamma[\,a\,]$-plots in Figure 5, where at late times each solution yields a Dark Energy dominated universe with $\Gamma[\,a\,](t) \to -1$ as $t \to \infty$. Moreover, $\Gamma[\,a\,]$ appears as approaching the Dark Energy value -1 similarly to how a damped harmonic oscillator reaches it stable equilibrium.

If, on the other hand, we approach $\varepsilon \to -\frac{1}{5760\pi^2}$ from below, the solutions tend to 0 for $t < 0$ and to infinity for $t > 0$ on always shorter time scales. These solutions are shown in the right graphic of Figure 5. Analogous graphs can be generated for any value ξ in the interval distinguished in Section 4, $|\xi - \frac{1}{6}| < \sqrt{1/4320}$.

Very similar observations have been made in [10]. There the authors approximate the state's contributions to the back-reaction equation, but also observe that the respective Starobinski solution $a(t) \propto \exp(H^{\text{dS}}t)$ is attractive if $\varepsilon - \varepsilon_{\text{crit}}$ has the correct sign, and is repulsive for the opposite sign.

The solutions shown in this section, at least for $\varepsilon > \varepsilon_{\text{crit}}(\xi = \frac{1}{6})$, underpin our observation of a late-time de Sitter expansion being generic.

5.2 Influence of the initial values

If we specify a certain interval of 'reasonable' q_0-values, we again end up with the generic solution class from Section 4, where the choice of q_0 adjusts the initial value of $\Gamma[\,a\,]$.

The left graphic of Figure 6 shows the transition from an (approximately) exponential expansion ($q_0 = -1$, curve (b)) to a square-root-like expansion ($q_0 = 1$, curve (j)). Still for $q_0 = -1$ (curve (b)) we observe a radiation-like expansion at very early times. The upper right graphic in Figure 6 shows the respective curves of $\Gamma[\,a\,]$. The lower right graphic shows a variation of curve (b) on a logarithmic scale. The Dark Energy dominated period is pushed to smaller values of a by increasing $\varepsilon = 3c_3 + c_4$, or k_1, respectively.

Curves (a) and (k) in Figure 6 show solutions with values for the deceleration parameter outside the interval $[-1, 1]$, namely for $q_0 = -2$ and $q_0 = 2$. On both sides of said interval we observe an inflection point with zero derivative, at $t < 0$ for $q_0 < -1$ and at $t > 0$ for $q_0 > 1$. Plotting more curves, one would, moreover, see convergence of this inflection point to $t = 0$ for both $q_0 \to \infty$ and $q_0 \to -\infty$ and in both these limits the solutions converge to the same function, now with an inflection point with zero derivative at $t = 0$. An inflection point with zero derivative of some a does imply a divergence of $\Gamma[\,a\,]$, which we can observe in the upper

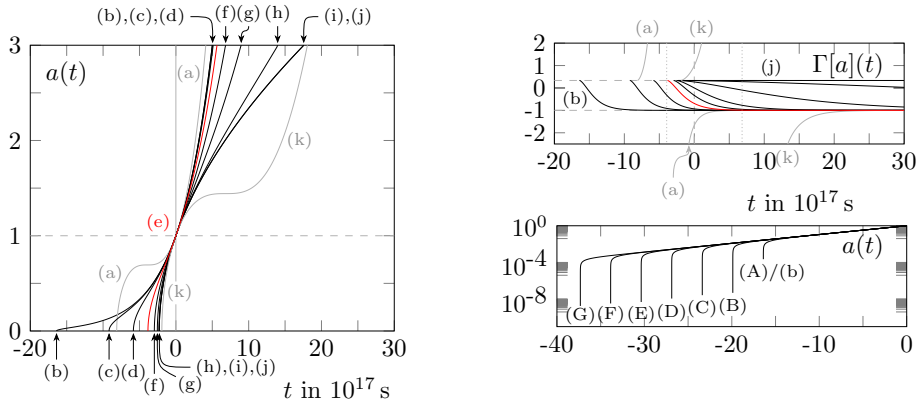

Figure 6: The left graphic shows several solutions with a varying deceleration parameter $q_0 \in [-1, 1]$ labeled by (a) to (k). The gray curves, (a) and (k), show solutions for q_0 outside that interval. On the right top we show the respective plots of $\Gamma[a]$. The unlabeled curves in said graphic belong to the parameters in the obvious order, that is between (b) and (j) we have (c) to (i) from left to right. The lower right graphic shows several solutions with $q_0 = -1$ in a logarithmic plot, showing how with an increasing value of ε the solutions better and better approximate a de Sitter solution, also at small values of a. Note that for these parameters a_{crit} is numerically infinite.

$\dot{a}(0) = H_0$ $\qquad \kappa = 2 \cdot 10^{42}$
$\lambda_0 = 1$ $\qquad \xi = \frac{1}{12}$

$\varepsilon = 1$:		$q_0 = -1$:	
(a)	$q_0 = -2$	(A)	$\varepsilon = 1$
(b)	$q_0 = -1$	(B)	$\varepsilon = 10$
(c)	$q_0 = -0.99$	(C)	$\varepsilon = 10^2$
(d)	$q_0 = -0.9$	(D)	$\varepsilon = 10^3$
(e)	$q_0 = -0.538$	(E)	$\varepsilon = 10^4$
(f)	$q_0 = 0$	(F)	$\varepsilon = 10^5$
(g)	$q_0 = 0.5$	(G)	$\varepsilon = 10^6$
(h)	$q_0 = 0.9$		
(i)	$q_0 = 0.99$		
(j)	$q_0 = 1$		
(k)	$q_0 = 2$		

right graphic of Figure 6.

5.3 Cosmic horizon problem

We shortly recall the definition of conformal time. For a FLRW-type space-time with scaling factor a, we reparameterize the time coordinate by $\tau(t) = \int_0^t \left(a(t')\right)^{-1} \mathrm{d}t'$ such that $g = a(\tau)^2(-\mathrm{d}\tau^2 + g_{\mathbb{R}^3})$ holds in these new coordinates. In conformal time, a causal connection of two space-time points is given, iff they are causally connected in Minkowski space-time. For a Big Bang-solution a with zero t_{BB} we define $\tau_{\text{BB}} := \tau(t_{\text{BB}})$.

The cosmic horizon problem concerns the extremely homogeneous state of the observable universe. If, in an universe given by $a(t)$, two observable regions with the same matter distribution are not causally connected, this would exclude a homogenizing process in the common causal past of both regions. One solution to the cosmic horizon problem is that *all* observable regions of the universe have a common causal past, which is achieved by a large negative value of τ_{BB} or even $\tau_{\text{BB}} = -\infty$. This is realized by theories of the inflationary early universe [19, 27, 28].

Here we want to investigate how much the cosmological model introduced here is compatible with solutions to the cosmic horizon problem. We observed in Section 5.1 that in specific regions of the parameter space the solutions $a(t)$ show an inflection point with vanishing first derivative, and we can even have arbitrarily many of them, see e.g. Figure 5 with $\varepsilon > \varepsilon_{\text{crit}}(\xi)$. Tuning ε

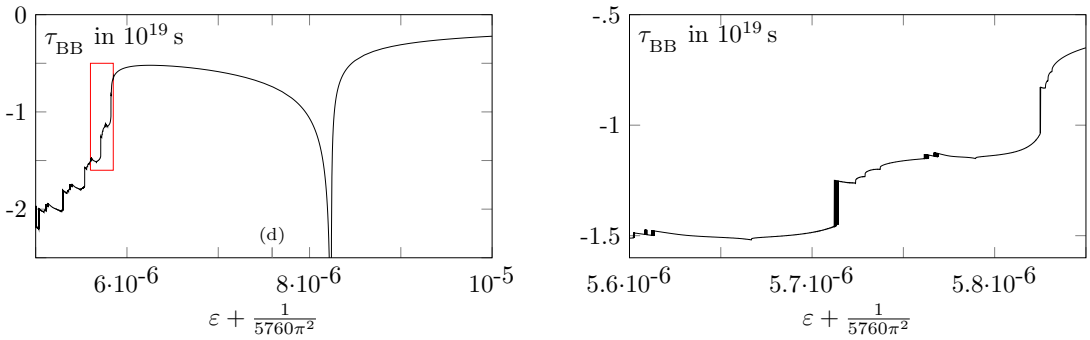

Figure 7: τ_{BB} as a function of ε or, more precisely, its deviation from the critical value (i.e. for which $\exp\left(\frac{k_1}{k_2}\right) = 1$), in the case $\xi = \frac{1}{6}$. The remaining parameters are set to the standard values from Section 4. The red box in left plot marks the plot area of the right graphic. The tick (d) marks the ε-value of curve (d) in Figure 5.

such that the inflection point coincides with the Big Bang, we obtain $\tau_{\mathrm{BB}} = -\infty$. Note that if we choose $\xi \neq \frac{1}{6}$ we need a value $\varepsilon > \varepsilon_{\mathrm{crit}}(\xi)$ such that $a_{\mathrm{crit}} > 1$, otherwise the solutions do not exist long enough to end in a Big Bang.

Figure 7 shows τ_{BB} as a function of $\varepsilon = 3c_3 + c_4$ for fixed $\xi = \frac{1}{6}$ and H_0, q_0, λ_0 and κ as in Section 4. We observe a divergence of τ_{BB} as expected. At the left end of the plot, edited as a zoom in the right panel, we observe several discontinuities. Comparing the respective numerical solutions we find that in each discontinuous step of τ_{BB} the solution gathers another inflection point. The thick-lined part shows a discontinuity where τ_{BB} jumps between two regions of continuity.

In the left graphic of Figure 8 we see the analog of Figure 7 for some values $\xi \neq \frac{1}{6}$. Our observations match the expectations, namely that also for $\xi \neq \frac{1}{6}$ (but still close to $\frac{1}{6}$) we observe an oscillatory behavior which results in several inflection points with zero first derivative which, if shifted to the $a = 0$-singularity by tuning ε, yields a divergence of τ_{BB}. The right panel shows this behavior as a function of both $\varepsilon - \varepsilon_{\mathrm{crit}}$ and ξ.

Such negative poles of τ_{BB} only exist up to a certain value of $|\xi - \frac{1}{6}|$ where the highest blue band (labelled Σ in Figure 8) in the right panel of Figure 8 meets the vertical axis on the left. Determining this value numerically, we find that for this ξ value $|\xi - \frac{1}{6}| = \sqrt{\frac{1}{4320}}$ (up to numerical error), that is, the maximum deviation of ξ from $\frac{1}{6}$ such that our trace equation possesses exact de Sitter solutions specified in Section 4. Recalling the discussion there, this is not surprising as the observed oscillations appear as decaying perturbations around the stable de Sitter solution.

To conclude, although the model introduced in this article *can* solve the cosmic horizon problem, fine tuning of the renormalization constants is required and the resulting cosmologies are not close to the ΛCDM cosmological standard model.

6 Comparison with numerical ΛCDM model solutions

In this section we want to compare our model's solutions to the ΛCDM model's solutions with the parameters $\Omega_{\mathrm{rad}} = 5.38 \cdot 10^{-5}$, $\Omega_{\mathrm{dust}} = 0.315$, $\Omega_{\mathrm{DE}} = 0.685$ and $H_0 = 2.2 \cdot 10^{-18}\,\frac{1}{\mathrm{s}}$ from [34]. For this purpose we fit our model's parameters to the ΛCDM solution using different measures of deviation. In this way, we obtain a rough idea of parameter regions of our model that produce 'reasonable' cosmologies, despite the fact that a detailed investigation would require the inclusion of massive fields an therefore goes beyond the scope of this paper.

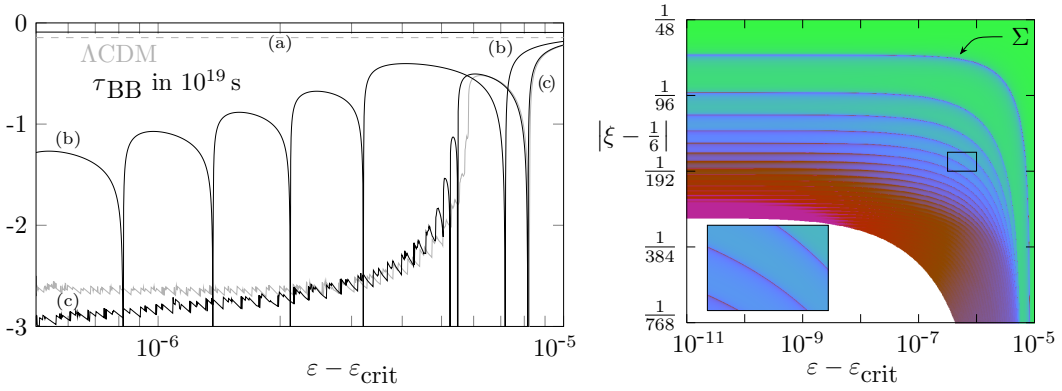

Figure 8: The left graphic shows τ_{BB} as a function of $\varepsilon - \varepsilon_{\mathrm{crit}}(\xi)$ for values close to, but not equal to, $\frac{1}{6}$ which are listed to the right. The background curve in gray shows the reference curve from Figure 7 with $\xi = \frac{1}{6}$. All remaining parameters are set to the standard values from Section 4. The gray dashed line marks the analog value of the ΛCDM model as discussed in Section 4. The right graphic shows τ_{BB}, now as a function of both $\varepsilon - \varepsilon_{\mathrm{crit}}(\xi)$ and ξ together with a zoom of the boxed area. For a later purpose, we label the top right connected set of poles of τ_{BB} by Σ.

(a) $\xi = \frac{1}{6} - \frac{1}{48}$
(b) $\xi = \frac{1}{6} - \frac{1}{192}$
(c) $\xi = \frac{1}{6} - \frac{1}{768}$

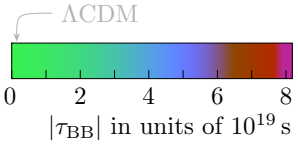

6.1 ΛCDM uncertainty band

The ΛCDM parameters come with uncertainty errors, namely the 1-σ uncertainties are given by (cf. [34])

$$\Omega_{\mathrm{rad}} = (5.38 \pm 0.15) \cdot 10^{-5}, \qquad \Omega_{\mathrm{dust}} = 0.315 \pm 0.007,$$
$$\Omega_{\mathrm{DE}} = 0.685 \pm 0.007, \qquad H_0 = (2.184 \pm 0.016) \cdot 10^{-18}\, \tfrac{1}{\mathrm{s}}.$$

Bounded by these errors we obtain a cuboid Q in the ΛCDM parameter space. For each $y \in Q$ we denote the respective ΛCDM solution by $a_{\Lambda\mathrm{CDM}}(y) : \mathbb{R} \to [0, \infty)$, wherefore we extend such a solution at the Big Bang and before by zero. By setting

$$a_{\max}(t) := \sup_{y \in Q} \big(a_{\Lambda\mathrm{CDM}}(y)\big)(t) \qquad \text{and} \qquad a_{\min}(t) := \inf_{y \in Q} \big(a_{\Lambda\mathrm{CDM}}(y)\big)(t),$$

we obtain an uncertainty band of the ΛCDM model in the t-a-plane that is compatible with 1-σ-errors in the single parameters.

As a numerical test of our model we want to determine a certain region of the ξ-ε-plane for fixed remaining parameters such that the solution a fulfills

$$a_{\min}(t) \leq a(t) \leq a_{\max}(t) \tag{31}$$

for all $t \in \mathbb{R}$, where we likewise extend our solutions by zero before a Big Bang.

For fixed H_0, q_0, λ_0 and κ as in Section 4, Figure 9 shows the region in the ξ-ε-plane where the solutions of our model fulfill (31). The shaded area in the left graphic of Figure 9 marks the parameter region where $\exp\left(\frac{k_1}{k_2}\right) \in \left[\frac{1}{3001}, 1\right]$ holds. The left bound of said interval corresponds to the upper parabola-shaped bound of the shaded region. The right bound in turn corresponds

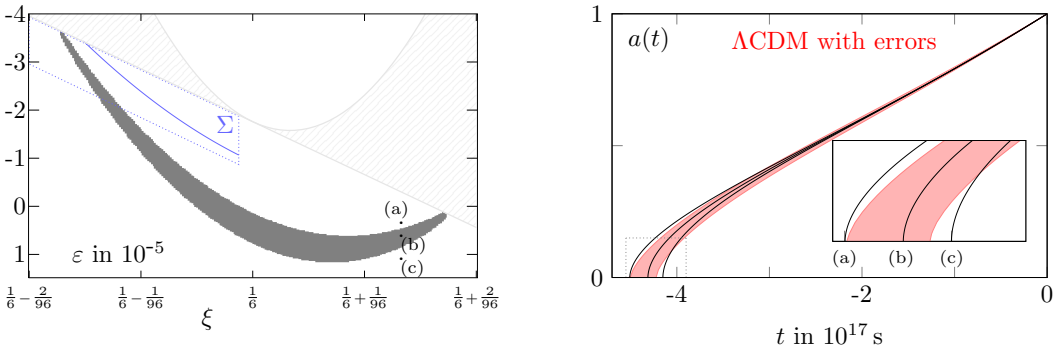

Figure 9: The gray area in the left graphic marks the ξ-ε-points in which the solution of the cSCE fulfills (31) for fixed remaining parameters as in Section 4. The shaded area marks ξ-ε-points for which $a_{\text{crit}} \in \left[\frac{1}{3001}, 1\right]$ holds. The points (a), (b) and (c) each mark an exemplary solution above, in and below the gray area, respectively. For orientation, the blue dotted parallelogram marks the boundaries of the right plot in Figure 8 and therein the blue line marks the set Σ. The right graphic illustrates our numerical test by showing the ΛCDM uncertainty band in the t-a-plane in red together with the solutions of the cSCE corresponding to the parameter points (a), (b) and (c).

to the linear lower bound of the shaded area, that is, it corresponds to $\varepsilon_{\text{crit}}(\xi)$.

As we can see, there exist parameters for which (31) holds. They form a hook-shaped subset, narrowly distributed around the conformally coupled case $\xi = \frac{1}{6}$ and around the respective $\varepsilon_{\text{crit}}(\xi)$. As mentioned before, our trace equation is symmetric under reflection at $\xi = \frac{1}{6}$ – if we additionally adjust ε. Hence, the gray area has a symmetric shape if we skew the graphic in a way such that the values of $\varepsilon_{\text{crit}}$ form a horizontal line. In the right graphic of Figure 9 we can see a visualization of the uncertainty band defined by (31) together with some sample curves. These show the three possibilities of the solutions fulfilling the first inequality of (31), the second one or both of them, depending on whether the corresponding parameter point is below, above or inside the hook-shaped area, respectively.

6.2 Best parameter fit

We next tune our model parameters in a way such that the solution is as close as possible to the ΛCDM solution.

The major difficulty which prevents us from defining distance simply by some L^p-norm ($p \geq 1$) is that the solutions of our models exist on variable intervals. We therefore define a distance function as follows. We first note that the ΛCDM solution is strictly monotonously increasing and continuous, hence invertible. Furthermore, the solutions of our model are invertible by the same argument, at least if we stay in the parameter regions of our 'generic solution shape' of Section 4. Thereby, we define the distance between the ΛCDM solution $a_{\Lambda\text{CDM}} : (t_{\text{BB},\Lambda\text{CDM}}\,, \infty) \to \mathbb{R}$ (with the parameters from Section 4) and a solution of our model $a = a(\xi, \varepsilon, \kappa, H_0, q_0) : (t_{\text{BB},(\xi,\varepsilon,\kappa,H_0,q_0)}, \infty) \to \mathbb{R}$ by

$$d_{M,p}(a, a_{\Lambda\text{CDM}}) := \left(\int_0^M \left| a^{-1}(\alpha) - a_{\Lambda\text{CDM}}^{-1}(\alpha) \right|^p \, \mathrm{d}\alpha \right)^{1/p}$$

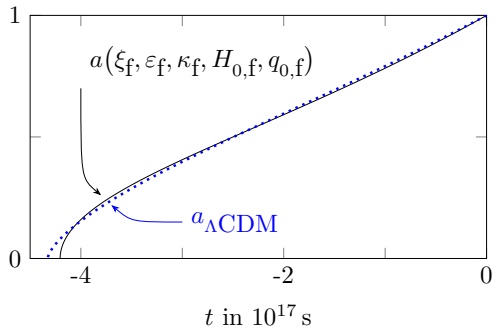

ξ_i	=	$\frac{1}{6}$
ε_i	=	1
κ_i	=	$2 \cdot 10^{42}$
$H_{0,i}$	=	$2.1975 \cdot 10^{-18} \frac{1}{s}$
$q_{0,i}$	=	-0.538
ξ_f	=	0.1651
ε_f	=	1.1152
κ_f	=	$2.6842 \cdot 10^{42}$
$H_{0,f}$	=	$2.3507 \cdot 10^{-18} \frac{1}{s}$
$q_{0,f}$	=	-0.7284

Figure 10: One (local) minimizer of (32) determined via a downhill simplex (Nelder-Mead) algorithm using the initial values Z_i on the right. The algorithm returned the values Z_f for which we see the solution on the left. As a reference the dotted line shows the ΛCDM solution.

with some $p \geq 1$ and some $M > 0$ such that a exists up to the value M. We solve the minimization problem

$$\min_{(\xi,\varepsilon,\kappa,H_0,q_0)} d_{M,p}\big(a(\xi,\varepsilon,\kappa,H_0,q_0), a_{\Lambda CDM}\big) \tag{32}$$

where $(\xi, \varepsilon, \kappa, H_0, q_0) \in \mathbb{R} \times \mathbb{R} \times \mathbb{R}_{>0} \times \mathbb{R}_{>0} \times \mathbb{R}$.

Note that since in this context we consider the ΛCDM as a representation of experimental data and they are obviously measured at times where $a \leq 1$ a value of $M = 1$ seems reasonable. Furthermore we choose $p = 2$ to suppress large deviations.

By our previous discussions we do not expect a unique minimum due to the symmetries of our trace equation under $\xi \mapsto \frac{1}{3} - \xi$ (and adjusting ε to obtain the same deviation from $\varepsilon_{crit}(\xi)$). Therewith, the minimum of course depends on the starting values for a downhill simplex algorithm. If the initial value of ε is greater than $\varepsilon_{crit}(\xi)$ (w.r.t the initial ξ) we would not expect the algorithm to be able to pass the $\varepsilon_{crit} = 0$-hypersurface[5] due to the behavior around these values we have presented in the previous sections. Also we would not expect the algorithm to pass the $\kappa = 0$ hypersurface for the same reason. Furthermore, we expect the deceleration parameter to remain in the interval $[-1, 1]$ of reasonable values, since otherwise the inflection points presented in Figure 6 fade in and yield a large $d_{M,p}$-distance for any choice of (M, p).

As a minimizer we find the parameters Z_f by using the exemplary initial values Z_i according to the table in Figure 10. The plot in Figure 10 shows the respective solution to our model together with the ΛCDM solution (blue dotted). As we expected, we end up with a value of ξ_f close to $\frac{1}{6}$, with a value of $\varepsilon_f \geq \varepsilon_{crit}(\xi_f)$ and a value $q_{0,f} \in [-1, 1]$. Also $H_{0,f}$ and κ_f remain close to $H_{0,i}$ and κ_i, respectively. Note that we only considered solutions with $\varepsilon > \varepsilon_{crit}$ such that $a_{crit} \in (0, 1)$ is avoided and $a(t)$ covers a-values in the entire interval $(0, 1)$.

6.3 The ΔN_{eff}-test

As one further method of comparing properties of our model to the respective properties of the ΛCDM model, we apply the ΔN_{eff}-test suggested by [22] as a procedure to obtain limits for parameters in the SCE, see [29, 30]. Following the literature, we reparameterize the FLRW

[5] Here we refer to the hypersurface in the space $\mathbb{R}_\xi \times \mathbb{R}_\varepsilon \times (\mathbb{R}_{>0})_\kappa \times (\mathbb{R}_{>0})_{H_0} \times \mathbb{R}_{q_0}$ parameterized by $(\xi, \varepsilon_{crit}(\xi)) \in \mathbb{R} \times \mathbb{R}$ with $\xi \in \mathbb{R}$ in the first coordinates and arbitrarily in the remaining coordinates.

space-time with scale factor $a(t)$ via the red shift factor

$$z(t) = \tfrac{1}{a(t)} - 1. \tag{33}$$

N_{eff} is the effective number of neutrino families, which can be related to Ω_{rad} in (29) via

$$\Omega_{\text{rad}} = \Omega_\gamma \left(1 + \frac{7}{8}\left(\frac{4}{11}\right)^{\frac{4}{3}} N_{\text{eff}}\right), \tag{34}$$

where Ω_γ is given by the energy content of photons in the present universe at $t = 0$. What is interesting for N_{eff} is the fact that from the observation of the cosmological microwave background (CMB) there are experimental values for N_{eff} that stem from the temperature spectrum of cosmic neutrinos in the CMB which slightly deviates from the thermal distribution. This deviation, in turn, can be computed from the energy distribution provided from a solution to the Boltzmann equation, in which the rate of expansion at the time of decoupling (between $z = 3000$ and $z = 1100$) enters [29, 30]. These calculations also derive the deviation from the number of neutrino families $N = 3$ and also the prefactor $\frac{7}{8}\left(\frac{4}{11}\right)^{\frac{4}{3}} = 0.2271$. These theoretical considerations also involve data from the Big Bang-nucleosynthesis (BBN) at $z \approx 10^9$, where the observed fraction of helium depends on the expansion rate. The experimental findings are well compatible with the theoretical prediction $N_{\text{eff}} = 3.046$, i.e. $N_{\text{eff}} = 3.36^{+0.68}_{-0.64}$ from the CMB power spectrum and $N_{\text{eff}} = 3.52^{+0.48}_{-0.45}$ at BBN with 95% confidence each, see [22, 37]. The theoretical value for N_{eff} along with $\Omega_{\text{rad}} = 5.38 \cdot 10^{-5}$ by (34) results in $\Omega_\gamma = 3.18 \cdot 10^{-5}$.

To connect N_{eff} to the rate of expansion, we define the difference of the squared normalized expansion rate to the theoretical prediction at the standard value for N_{eff} as

$$\delta\left(\frac{H}{H_0}\right)^2(z) := \frac{1}{a(z)^2}\frac{\dot{a}(z)^2}{\dot{a}(0)^2} - \Omega_{\text{DE}} - \Omega_{\text{dust}}(1+z)^3 - \Omega_{\text{rad}}(1+z)^4, \tag{35}$$

where in $\dot{a}(z)$ we first take the derivative with respect to t and then reparameterize by (33).

Following [22], we define $\Delta N_{\text{eff}} = N_{\text{eff}} - 3.046$ as the deviation of N_{eff} from the theoretical value given in [29, 30]. Now we can express the difference between the squared and normalized expansion rate $\left(\frac{H}{H_0}\right)^2(z)$ at the red shift parameter z via ΔN_{eff} and obtain

$$\Delta N_{\text{eff}}(z) = \frac{1}{\Omega_\gamma}\frac{\delta\left(\frac{H}{H_0}\right)^2(z)}{0.2271(1+z)^4}. \tag{36}$$

This parametrization of the observed difference in expansion can now be used to check, whether the error bounds, roughly $|\Delta N_{\text{eff}}| \lesssim 1$ are fulfilled. As the BBN red shift for $z = 10^9$ is hard to achieve numerically, we restict to the CMB case and determine $\Delta N_{\text{eff}}(z = 3000)$ as a function of the model parameters numerically. $z = 10^9$ for the BBN is beyond the capabilities of our solver.

To this purpose, we plot ΔN_{eff} as a function of our parameters. Hereby, we restrict ourselves to the ξ - ε plane and fix the remaining parameters as in Section 4.

Figure 11 shows $\Delta N_{\text{eff}}(z = 3000)$ as a function of ξ and ε for points (ξ, ε) in which $a_{\text{crit}} \notin \left[\frac{1}{3001}, 1\right]$. Again, the diagonal straight line marks $\varepsilon_{\text{crit}}(\xi)$ and if we skewed that line to be horizontal we would end up with a graphic that is symmetric with respect to reflection at $\xi = \frac{1}{6}$. On the other hand, the parabola shaped upper bound of the shaded area corresponds to $a_{\text{crit}} = \frac{1}{3001}$. In the shaded area, our solution does not reach $z = 3000$ and the ΔN_{eff}-test does not make sense. In the left graphic of the figure we included the parameter region from Figure 9. We find a small region where ΔN_{eff} is smaller than the experimental error of 0.5 around

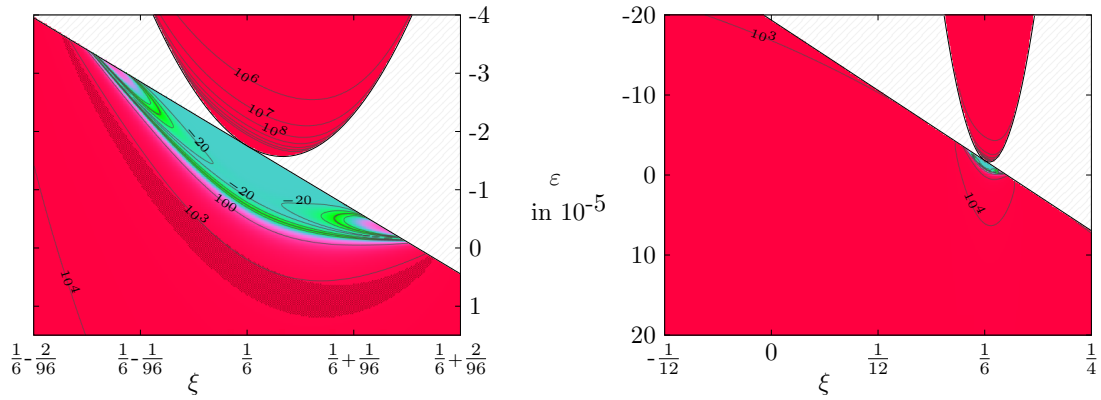

Figure 11: $\Delta N_{\text{eff}}(z = 3000)$ as a function of ξ and ε for fixed remaining parameters as in Section 4. The gray shaded area marks the parameter region where $\exp\left(\frac{k_1}{k_2}\right) \in \left[\frac{1}{3001}, 1\right]$ and hence $\Delta N_{\text{eff}}(3000)$ does not exist. The colors are determined from the absolute value of $\Delta N_{\text{eff}}(3000)$ and we emphasize the sign change along the green stripe, particularly there exists a curve whereon $\Delta N_{\text{eff}}(3000) = 0$. For orientation, the dashed area in the left graphic marks the parameter region represented in Figure 9.

$\xi = \frac{1}{6}$ and for rather small deviations of ε from $\varepsilon_{\text{crit}}$. An interesting feature of this graphic is that the level sets of $\Delta N_{\text{eff}}(3000)$ is not too far away from the grey shaded region passing the test of Section 6.1. Despite the fact that this region fails to pass the ΔN_{eff} test by three orders of magnitude, one should keep in mind that our reduced model can only give a qualitative and preliminary insight into semiclassical cosmology.

As a main takeaway from this section, the ΔN_{eff} seems to favour the region of small ε and ξ close to the case of conformal coupling $\xi = \frac{1}{6}$.

Remark 6. *Another remarkable alignment is found between the present numerical test and the regions of a divergent τ_{BB} from Section 5.3. The poles labeled by the set Σ apparently match with the $\Delta N_{\text{eff}}(3000) = 0$-level set quite well.*

7 Conclusion and Outlook

In this work we investigated cosmological solutions of the SCE for massless quantum fields in special Minkowski-like states. In such states, the dynamical degrees of freedom from the scale factor decouple from the dynamics of the quantum state, as such states come with a vanishing 'tower of moments' in the sense of [18]. While this phenomenon was well known in the conformally coupled case [40], we here observe some new cases that also include non conformally coupled fields. We thus retrieve new cosmological models from the solutions of the massless SCE.

We provided a detailed numerical study of these new cosmological models. Typical solutions show a radiation like Big Bang in the early universe in conjunction with a Dark Energy-like behavior for the late universe. In our models, the late time universe Dark Energy phase is observed without introducing a cosmological constant, neither directly nor through a renormalization constant. Such models expose a smooth transition in the state equation connection energy and pressure that ranges from the ratio $\frac{1}{3}$ (radiation) to -1 (Dark Energy).

We also investigate special parameter settings that give rise to a solution of the cosmological horizon problem as proposed by [35]. While we give numerical evidence that such solutions

exist, we also see that this behavior requires parameter tuning and is not stable under small parameter variations.

A large part of this work is concerned with a numerical comparison of our cosmological models with the ΛCDM standard model of cosmology. Evidently, we observe deviations in the cold dark matter dominated phase of ΛCDM cosmology, which in turn is to be expected for a massless quantum field. We however show that a parameter fit of our cosmological models to the ΛCDM cosmology endowed with physical parameters [37] remains in the strip of observational 1-σ-uncertainty of the ΛCDM model. Also, we identify 'physical' parameter regions that comply with the ΔN_{eff}-test as suggested by [22]. Despite that both parameter regions do not have an intersection, they are positioned close to each other in parameter space. Interestingly, these tests seem to favour coupling ξ close to conformal coupling $\xi = \frac{1}{6}$ rather than minimal coupling $\xi = 0$ and a small value of the renormalization constant $\varepsilon = 3c_3 + c_4$.

While we have gathered evidence that semi-classical cosmology, even without cosmological constant, can produce interesting cosmologies that are not too far from the standard cosmology, further extension and refinement of the model seems to be in order. Obviously, massive fields should be incorporated and also fields with higher spin and Fermi statistics [20].

Some scholars also object the higher order nature of the SCE which involves up to fourth order derivatives in the scale factor $a(t)$. Therefore it would, moreover, be of interest to derive the corresponding second order equations via the procedure of self-consistent order reduction as suggested by Parker and Simon [33] and study the resulting cosmological models.

Acknowledgement.
The authors thank T. P. Hack, N. Pinamonti and P. Meda for interesting discussions.

References

[1] R. P. Agarwal and D. O'Regan. *An introduction to ordinary differential equations*. Springer Science & Business Media, 2008.

[2] P. R. Anderson. Effects of quantum fields on singularities and particle horizons in the early universe. *Phys. Rev. D*, 28:271–285, 1983.

[3] P. R. Anderson. Effects of quantum fields on singularities and particle horizons in the early universe. 2. *Phys. Rev. D*, 29:615–627, 1984.

[4] P. R. Anderson. Effects of quantum fields on singularities and particle horizons in the early universe. 3. The conformally coupled massive scalar field. *Phys. Rev. D*, 32:1302, 1985.

[5] P. R. Anderson. Effects of quantum fields on singularities and particle horizons in the early universe. 4. Initially empty universes. *Phys. Rev. D*, 33:1567, 1986.

[6] J. D. Barrow and S. Cotsakis. Inflation and the conformal structure of higher-order gravity theories. *Phys. Lett. B*, 214(4):515–518, 1988.

[7] N. D. Birrell and P. C. W. Davies. *Quantum fields in curved space*. Cambridge University Press, 1984.

[8] T. S. Bunch and P. C. W. Davies. Quantum field theory in de Sitter space: renormalization by point-splitting. *Proc. R. Soc. Lond. A.*, 360(1700):117–134, 1978.

[9] C. Dappiaggi, K. Fredenhagen, and N. Pinamonti. Stable cosmological models driven by a free quantum scalar field. *Phys. Rev. D*, 77(10):104015, 2008.

[10] C. Dappiaggi, T.-P. Hack, J. Moller, and N. Pinamonti. Dark energy from quantum matter. *arXiv:1007.5009 [astro-ph.CO]*, 2010.

[11] J. Dimock. Algebras of local observables on a manifold. *Commun. Math. Phys.*, 77(3):219–228, 1980.

[12] J. Dimock and B. S. Kay. Classical wave operators and asymptotic quantum field operators on curved space-times. *Annales de l'IHP Physique théorique*, 37(2):93–114, 1982.

[13] B. Eltzner and H. Gottschalk. Dynamical backreaction in Robertson–Walker spacetime. *Rev. Math. Phys.*, 23(05):531–551, 2011.

[14] E. E. Flanagan. Higher-order gravity theories and scalar-tensor theories. *Class. Quantum Gravity*, 21(2):417, 2003.

[15] K. Fredenhagen and T.-P. Hack. Quantum field theory on curved spacetime and the standard cosmological model. *Lect. Notes Phys.*, 899:113–129, 2013.

[16] S. A. Fulling et al. *Aspects of quantum field theory in curved spacetime*, volume 17. Cambridge university press, 1989.

[17] H. Gottschalk, N. Rothe, and D. Siemssen. Cosmological de Sitter solutions of the semiclassical Einstein equation. *to be published.*

[18] H. Gottschalk and D. Siemssen. The cosmological semiclassical Einstein equation as an infinite-dimensional dynamical system. *Ann. Henri Poincaré*, 22(12):3915–3964, 2021.

[19] A. H. Guth. Inflationary universe: a possible solution to the horizon and flatness problems. *Phys. Rev. D*, 23:347–356, 1981.

[20] T.-P. Hack. *On the backreaction of scalar and spinor quantum fields in curved spacetimes.* PhD thesis, Universität Hamburg, Institut für Theoretische Physik II, 2010.

[21] T.-P. Hack. The LambdaCDM-model in quantum field theory on curved spacetime and dark radiation. *arXiv:1306.3074 [gr-qc]*, 2013.

[22] T.-P. Hack. *Cosmological applications of algebraic quantum field theory in curved spacetimes.* Springer, 2016.

[23] M. Hänsel. *Qualitative analysis of solutions to the semiclassical Einstein equation inhomogeneous and isotropic spacetimes.* PhD thesis, Universität Leipzig, 2019.

[24] S. Hollands and R. M. Wald. Conservation of the stress tensor in interacting quantum field theory in curved spacetimes. *Rev. Math. Phys.*, 17:227–312, 2005.

[25] B. A. Juárez-Aubry. Semi-classical gravity in de Sitter spacetime and the cosmological constant. *Phys. Lett. B*, 797:134912, 2019.

[26] B. A. Juárez-Aubry. Semiclassical gravity in static spacetimes as a constrained initial value problem. *arXiv:2011.05947 [gr-qc]*, 2020.

[27] A. R. Liddle. An introduction to cosmological inflation. In A. Masiero, G. Senjanović, and A. Smirnov, editors, *1998 Summer School in High-Energy Physics and Cosmology*, pages 260–295. World Scientific, 1999.

[28] A. D. Linde. A new inflationary universe scenario: a possible solution of the horizon, flatness, homogeneity, isotropy and primordial monopole problems. *Phys. Lett. B*, 108(6):389–393, 1982.

[29] G. Mangano, G. Miele, S. Pastor, and M. Peloso. A precision calculation of the effective number of cosmological neutrinos. *Phys. Lett. B*, 534(1-4):8–16, 2002.

[30] G. Mangano, G. Miele, S. Pastor, T. Pinto, O. Pisanti, and P. D. Serpico. Relic neutrino decoupling including flavour oscillations. *Nucl. Phys. B*, 729(1-2):221–234, 2005.

[31] P. Meda, N. Pinamonti, and D. Siemssen. Existence and uniqueness of solutions of the semiclassical Einstein equation in cosmological models. *Ann. Henri Poincaré*, 22:3965–4015, 2021.

[32] V. Moretti. Comments on the stress energy tensor operator in curved space-time. *Commun. Math. Phys.*, 232:189–221, 2003.

[33] L. Parker and J. Z. Simon. Einstein equation with quantum corrections reduced to second order. *Phys. Rev. D*, 47(4):1339, 1993.

[34] Particle Data Group. Astrophysical constants and parameters. Available at https://pdg.lbl.gov/2020/reviews/rpp2020-rev-astrophysical-constants.pdf, 2020.

[35] N. Pinamonti. On the initial conditions and solutions of the semiclassical Einstein equations in a cosmological scenario. *Commun. Math. Phys.*, 305(3):563–604, 2011.

[36] N. Pinamonti and D. Siemssen. Global existence of solutions of the semiclassical Einstein equation for cosmological spacetimes. *Commun. Math. Phys.*, 334(1):171–191, 2015.

[37] Planck Collaboration, N. Aghanim, Y. Akrami, M. Ashdown, J. Aumont, C. Baccigalupi, M. Ballardini, A. J. Banday, R. B. Barreiro, N. Bartolo, et al. Planck 2018 results. VI. Cosmological parameters. *Astron. Astrophys.*, 641:A6, 2020.

[38] M. J. Radzikowski. Micro-local approach to the Hadamard condition in quantum field theory on curved space-time. *Commun. Math. Phys.*, 179(3):529–553, 1996.

[39] S. Schander and T. Thiemann. Backreaction in cosmology. *arXiv:2106.06043 [gr-qc]*, 2021.

[40] A. A. Starobinsky. A new type of isotropic cosmological models without singularity. *Phys. Lett. B*, 91:99–102, 1980.

[41] R. M. Wald. Asymptotic behavior of homogeneous cosmological models in the presence of a positive cosmological constant. *Phys. Rev. D*, 28:2118–2120, 1983.

[42] R. M. Wald. *Quantum field theory in curved spacetime and black hole thermodynamics*. University of Chicago Press, 1994.